Impact of sampling volume on the probability density function of steady state concentration

Ronnie L. Schwede,[1,2] Olaf A. Cirpka,[1,2] Wolfgang Nowak,[3] and Insa Neuweiler[4,5]

Received 15 November 2007; revised 23 May 2008; accepted 4 September 2008; published 23 December 2008.

[1] In recent years, statistical theory has been used to compute the ensemble mean and variance of solute concentration in aquifer formations with second-order stationary velocity fields. The merit of accurately estimating the mean and variance of concentration, however, remains unclear without knowing the shape of the probability density function (pdf). In a setup where a conservative solute is continuously injected into a domain, the concentration is bounded between zero and the concentration value in the injected solution. At small travel distances close to the fringe of the plume, an observation point may fall into the plume or outside, so that the statistical concentration distribution clusters at the two limiting values. Obviously, this results in non-Gaussian pdf's of concentration. With increasing travel distance, the lateral plume boundaries are smoothed, resulting in increased probability of intermediate concentrations. Likewise, averaging the concentration in a larger sampling volume, as typically done in field measurements, leads to higher probabilities of intermediate concentrations. We present semianalytical results of concentration pdf's for measurements with point-like or larger support volumes based on stochastic theory applied to stationary media. To this end, we employ a reversed auxiliary transport problem, in which we use analytical expressions for first and second central spatial lateral moments with an assumed Gaussian pdf for the uncertainty of the first lateral moment and Gauss-like shapes in individual cross sections. The resulting concentration pdf can be reasonably fitted by beta distributions. The results are compared to Monte Carlo simulations of flow and steady state transport in 3-D heterogeneous domains. In both methods the shape of the concentration pdf changes with distance to the contaminant source: Near the source, the distribution is multimodal, whereas it becomes a unimodal beta distribution far away from the contaminant source. The semianalytical and empirical pdf's differ slightly, which we contribute to the numerical artifacts in the Monte Carlo simulations but also to hard assumptions made in the semianalytical approach. Our results imply that geostatistical techniques for interpolation and other statistical inferences based on Gaussian distributions, such as kriging and cokriging, may be feasible only far away from the contaminant source. For calculations near the source, the beta-like distribution of concentration should be accounted for.

Citation: Schwede, R. L., O. A. Cirpka, W. Nowak, and I. Neuweiler (2008), Impact of sampling volume on the probability density function of steady state concentration, *Water Resour. Res.*, *44*, W12433, doi:10.1029/2007WR006668.

1. Introduction

[2] It is well accepted that natural aquifers exhibit strong variability of hydraulic conductivity, leading to high variability of dependent quantities [e.g., *Rubin*, 2003]. In many studies, the variability of the hydraulic conductivity field has been mathematically modeled as a random field. Hence, all dependent quantities are random variables too, namely, hydraulic heads, groundwater velocity, and concentrations of dissolved compounds. Statistical moments of heads and velocities have been derived by first-order methods in stationary fields [*Bakr et al.*, 1978; *Gutjahr et al.*, 1978] and in nonstationary fields [*Li and McLaughlin*, 1991, 1995], by higher-order approximations [*Neuman and Orr*, 1993; *Zhang and Lu*, 2004] and numerical simulations [*Zhang*, 1998; *Lu and Zhang*, 2004]. *Nowak et al.* [2008] investigated also the complete distribution of heads and velocities, showing significant non-Gaussian behavior of velocity. The latter authors argued that known bounds of distributions (e.g., upper and lower limit of hydraulic head in a source-free flow field with fixed head boundary conditions) should be considered when choosing parametric models for the pdf's of dependent quantities.

[3] Traditional stochastic analysis of solute transport in heterogeneous aquifers has dealt with spatial moments of

[1]Eawag, Swiss Federal Institute of Aquatic Science and Technology, Dübendorf, Switzerland.
[2]Now at Center for Applied Geoscience, University of Tübingen, Tübingen, Germany.
[3]Department of Civil and Environmental Engineering, University of California, Berkeley, California, USA.
[4]Institut für Wasserbau, Universität Stuttgart, Stuttgart, Germany.
[5]Now at Institut für Strömungsmechanik, Leibniz Universität Hannover, Hannover, Germany.

0043-1397/08/2007WR006668$09.00

the ensemble mean concentration [*Dagan*, 1984; *Neuman et al.*, 1987; *Gelhar and Axness*, 1983]. Assuming a particular shape of the spatial distribution (usually a Gaussian one) leads to the expected value of concentration at a particular location in space and time. *Kitanidis* [1988] realized that the second central spatial moments of the ensemble mean concentration can be separated into two contributions: the expected value of the second central spatial moments in single realizations, and the uncertainty of the first spatial moment. The rate of change of the first quantity can be described by effective dispersion, while ensemble dispersion describes how the second central spatial moments of the mean concentration increases. *Dentz et al.* [2000a, 2000b] derived closed form expressions of effective dispersion in stationary velocity fields using Eulerian methods. *Fiori and Dagan* [2000] came to the same expressions following a Lagrangian approach.

[4] *Kapoor and Gelhar* [1994] derived a transport equation for the concentration variance using an Eulerian perturbation approach. Unfortunately, the expression contained terms that are difficult to evaluate by analytical means. *Fiori and Dagan* [2000] computed the concentration variance from one- and two-particle displacements using first-order analytical expressions for the latter and assuming Gaussian distributions in space. More accurate methods of computing the mean concentration were presented by *Neuman* [1993] solving integro-differential equations. *Liu et al.* [2007] used a polynomial chaos expansion approach to achieve higher-order approximations of the concentration mean and variance.

[5] Without information about the shape of the statistical distribution, the worth of the concentration mean and variance is limited in many applications. In risk analysis, the exceedance probability of a given concentration may be of interest, which cannot be computed without knowing (or at least assuming) the shape of the concentration probability density function (pdf). Recently, *Cirpka and Valocchi* [2007] and *De Simoni et al.* [2007], among others, have presented methods of mapping conservative tracer concentrations to those of reactive species. The relationship between these concentrations is fairly nonlinear. Hence, an erroneous assumption about the pdf shape of conservative compound concentrations will lead to a wrong shape of the statistical distribution of a corresponding reactive species. It may even lead to biased metrics such as the mean and variance [*Cirpka et al.*, 2008]. Finally, common geostatistical methods of interpolation and inverse modeling, namely, kriging and cokriging-like techniques, are based on the implicit assumption of a Gaussian distribution [e.g., *Kitanidis*, 1995]. Strong deviations from a Gaussian distribution complicates the use of concentration measurements in statistical inference.

[6] To the best of our knowledge, *Fiorotto and Caroni* [2002], *Caroni and Fiorotto* [2005], and *Bellin and Tonina* [2007] present the only studies on the full pdf of solute concentration in heterogeneous media. The former authors estimated the pdf of point-like concentration measurements using first-order approximations of the one- and two-particle (co)variance of displacement [*Fiori and Dagan*, 2000] and assuming a Gaussian distribution of the displacement. These estimates were compared to Monte Carlo simulations using the particle-tracking random walk technique. The derived concentration pdf could be parameterized quite well by beta distributions. Particularly at short travel distances, the concentration pdf was bimodal, with high probabilities of very low and very high concentrations. *Bellin and Tonina* [2007] analytically derived the beta distribution assuming that the local concentration can be described by an Ito stochastic ordinary differential equation, containing a term linearly dampening deviations from the expected value of concentration, and a Wiener noise term that is maximal at intermediate concentrations.

[7] In field measurements, concentrations are typically not measured at points but in samples of a finite volume. Some sampling protocols require exchanging a certain number of well volumes before sampling, e.g., in order to exclude bias of the samples due to contact to air (degassing, oxidation). *Beckie* [1996], *Graham et al.* [1998], *Andričević* [1998], and *Rubin et al.* [1999], for example, showed that enlarging the sampling volume acts as smoothing mechanism on the concentration fluctuations. Graphically spoken, a sampling process with a nonzero support volume constitutes a mixing process of its own. This sampling-induced mixing, however, must not be confused with mixing within the formation. By enlarging the sampling volume, solute spreading, representing irregular plume shapes, becomes inseparable from in situ solute mixing representing the occurrence of local concentrations at intermediate values [e.g., *Cirpka and Kitanidis*, 2000]. It is suggestive that spatial averaging by sampling has similar effects on the concentration pdf as enhanced pore-scale dispersion. Namely, the pronounced bimodal shape should disappear and eventually a more Gaussian-like distribution might be obtained. The latter would make concentration measurements better suitable for (co)kriging-like methods of statistical inference, compared to what the strongly bimodal concentrations found by *Fiorotto and Caroni* [2002] and *Caroni and Fiorotto* [2005] would imply.

[8] In the present study, we analyze the effect of sampling volume on the concentration probability density function. We present a semianalytical approach of estimating the concentration pdf based on first-order stochastic theory applied to spatial moments which is conceptually similar to that of *Fiorotto and Caroni* [2002] and *Caroni and Fiorotto* [2005] but formulated in an Eulerian framework. The semianalytical results are compared to those obtained by extensive Monte Carlo simulations using Finite Element methods (FEM). It may be worth noting that approaches of computing full statistical distributions of concentration have some tradition in turbulence research [e.g., *Pope*, 1985]. In turbulent flows, however, the erratic fluctuations of flow vary in time, so that the full statistical distributions of velocity, pressure and concentration can be sampled by high-resolution measurements over a sufficiently long time period. This is different in groundwater flow in heterogeneous formations. Here, the fluctuations occur only in space, and the statistical distribution of concentration mainly reflects the inability of characterizing all details of the formation.

[9] The approach presented by *Fiorotto and Caroni* [2002] and *Caroni and Fiorotto* [2005] is based on first-order one- and two-particle statistics of displacement. Within this framework considering an extended sampling volume is cumbersome, because the approach requires integrating the two-particle covariance of displacement over all possible combinations of two points in the sampling

volume. In our formulation these integrations are not necessary.

[10] We restrict our analysis to steady state concentration mimicking the situation of a plume originating from a continuous source.

2. Governing Equation

[11] Steady state transport of a conservative, nonsorbing solute with concentration c in groundwater can be described by the advection-dispersion equation

$$\boldsymbol{\nabla} \cdot (\boldsymbol{v}c - \boldsymbol{D}\boldsymbol{\nabla}c) = 0 \text{ on } \Omega \tag{1}$$

subject to the boundary conditions:

$$\begin{aligned} \boldsymbol{n} \cdot (\boldsymbol{v}c - \boldsymbol{D}\boldsymbol{\nabla}c) &= \boldsymbol{n} \cdot \boldsymbol{v}c_{in} \quad \text{on} \quad \Gamma_{\text{in}} \\ \boldsymbol{n} \cdot (\boldsymbol{D}\boldsymbol{\nabla}c) &= 0 \qquad \text{on} \quad \Gamma_{\text{out}} \cup \Gamma_{\text{no}} \end{aligned} \tag{2}$$

with the seepage velocity $\boldsymbol{v}$, the local dispersion tensor $\boldsymbol{D}$, and the normal vector $\boldsymbol{n}$. The domain is denoted by Ω with boundary $\Gamma = \Gamma_{\text{in}} \cup \Gamma_{\text{out}} \cup \Gamma_{\text{no}}$, in which Γ_{in} is the boundary for which we assume a given function of inflow concentration c_{in}, Γ_{out} is a free outflow, and Γ_{no} a no-flow boundary. In the examples given below, c_{in} will be unity within a rectangle of size $L_2 \times L_3$ centered about the origin, and zero outside.

[12] The seepage velocity $\boldsymbol{v}$, appearing in the transport equation (1) is given by:

$$\boldsymbol{v} = \frac{\boldsymbol{q}}{\theta} = -\frac{K}{\theta}\boldsymbol{\nabla}h \tag{3}$$

in which $\boldsymbol{q}$ is the specific discharge, θ is the porosity, K is the hydraulic conductivity, and h is the hydraulic head meeting the steady state groundwater flow equation without internal sources and sinks:

$$-\boldsymbol{\nabla} \cdot (K\boldsymbol{\nabla}h) = 0 \text{ on } \Omega. \tag{4}$$

We set Dirichlet boundary conditions on the inflow and outflow of the domain and no-flow Neumann conditions on the other boundaries:

$$\begin{aligned} h &= h_{\text{in}} \quad \text{on} \quad \Gamma_{\text{in}} \\ h &= h_{\text{out}} \quad \text{on} \quad \Gamma_{\text{out}} \\ \boldsymbol{n} \cdot (K\boldsymbol{\nabla}h) &= 0 \quad \text{on} \quad \Gamma_{\text{no}} \end{aligned} \tag{5}$$

for given functions h_{in} and h_{out}.We assume that the log-hydraulic conductivity is a second-order stationary field:

$$K(\boldsymbol{x}) = K_g \exp(Y'(\boldsymbol{x})), \tag{6}$$

in which $\boldsymbol{x}$ is the vector of spatial coordinates, K_g is the spatially uniform geometric mean of $K(\boldsymbol{x})$, and $Y'(\boldsymbol{x})$ is a random Gaussian spatial variable with zero mean and covariance function $R_{Y',Y'}(\boldsymbol{x}, \boldsymbol{z})$ depending only on the distance $|\boldsymbol{x} - \boldsymbol{z}|$:

$$\begin{aligned} R_{Y',Y'}(\boldsymbol{x},\boldsymbol{z}) &= \mathrm{E}\left[Y'(\boldsymbol{x})Y'(\boldsymbol{z})\right] \\ &= R_{Y',Y'}(|\boldsymbol{x}-\boldsymbol{z}|)\ \forall \boldsymbol{x},\boldsymbol{z}, \end{aligned} \tag{7}$$

in which E[·] denotes the expected value of the argument.

[13] Because K is a random space variable, all dependent quantities i.e., h, $\boldsymbol{v}$, and c are random, too. Only if the relationship between $\ln(K)$ and the concentration was linear, the pdf of c would be Gaussian. This, however, is not the case because the governing equations, equations (1), (3), and (4), involve products of the random variables. *Englert et al.* [2006] and *Nowak et al.* [2008] showed that already the velocity components deviate from Gaussian variables. Even if $\boldsymbol{v}$ was Gaussian, as assumed in various stochastic analytical approaches [e.g., *Neuman*, 1993; *Fiori and Dagan*, 2000], the statistical distribution of concentration c could not be Gaussian. The simplest proof of non-Gaussian behavior is that the statistical distribution of c is bounded, whereas the Gaussian distribution is not.

3. Approach and Methods

3.1. Sampling of Concentration Measurements

[14] Concentrations are seldom measured at ideal points. Typically, samples are pumped from observation wells screened over a certain depth range. As shown by *Andričević* [1998], among others, the statistical moments of concentration depend on the sampling volume (SV) because spreading and plume meandering have a big effect on point-like measurements but only a minor one on averages over larger cross sections.

[15] In the current study, we consider measurements of concentration in a cross-sectional layer, implying averaging over a sampling area rather than a volume; that is, the concentration is averaged in the two transverse directions but not along the main flow direction. The averaging is done by applying a rectangular filter function, that is, we compute the arithmetic mean concentration in the sampling area [e.g., *Fiori et al.*, 2002]. Within the framework of steady state transport considered in our study, variability of concentration along the longitudinal direction is much smaller than along the transverse directions, so that the restriction of sampling volumes to cross-sectional areas is relatively insignificant.

[16] The concentration measurement may either be in terms of the resident or flux concentration. The resident concentration (denoted by superscript "r") observed in the sampling area described by the sampling function χ is given by the arithmetic average of concentration:

$$c^r_{\text{obs}} = \int_\Omega \chi\left(\boldsymbol{x}_{2,3} - \boldsymbol{x}^{obs}_{2,3}\right)\delta\left(x_1 - x^{obs}_1\right)c(\boldsymbol{x}|c_{\text{in}}(\boldsymbol{x}'))\,\mathrm{d}\boldsymbol{x} \tag{8}$$

in which $\delta(\cdot)$ is the Dirac delta function, and $c(\boldsymbol{x}|c_{\text{in}}(\boldsymbol{x}'))$ expresses that the spatial concentration distribution in the domain depends on the spatial distribution of the inflow concentration in the injection plane. $\boldsymbol{x}'$ denotes the spatial coordinate within the injection plane and is explicitly needed later on. Here and in the following we denote elements of vectors with subscript numbers, e.g., $\boldsymbol{x} = (x_1, x_2, x_3)$ and we use two numbers as subscripts to define a new vector with only these two entries, e.g., $\boldsymbol{x}_{2,3} = (x_2, x_3)$.

[17] In the present study, we consider sampling over a rectangle with dimensions $w_2 \times w_3$, implying for the sampling function χ:

$$\chi(\boldsymbol{h}_{2,3}) = \begin{cases} \dfrac{1}{w_2 w_3} & \text{if} \quad -w_2/2 \le h_2 \le w_2/2 \quad \text{and} \\ & \quad -w_3/2 \le h_3 \le w_3/2 \\ 0 & \text{else} \end{cases} \tag{9}$$

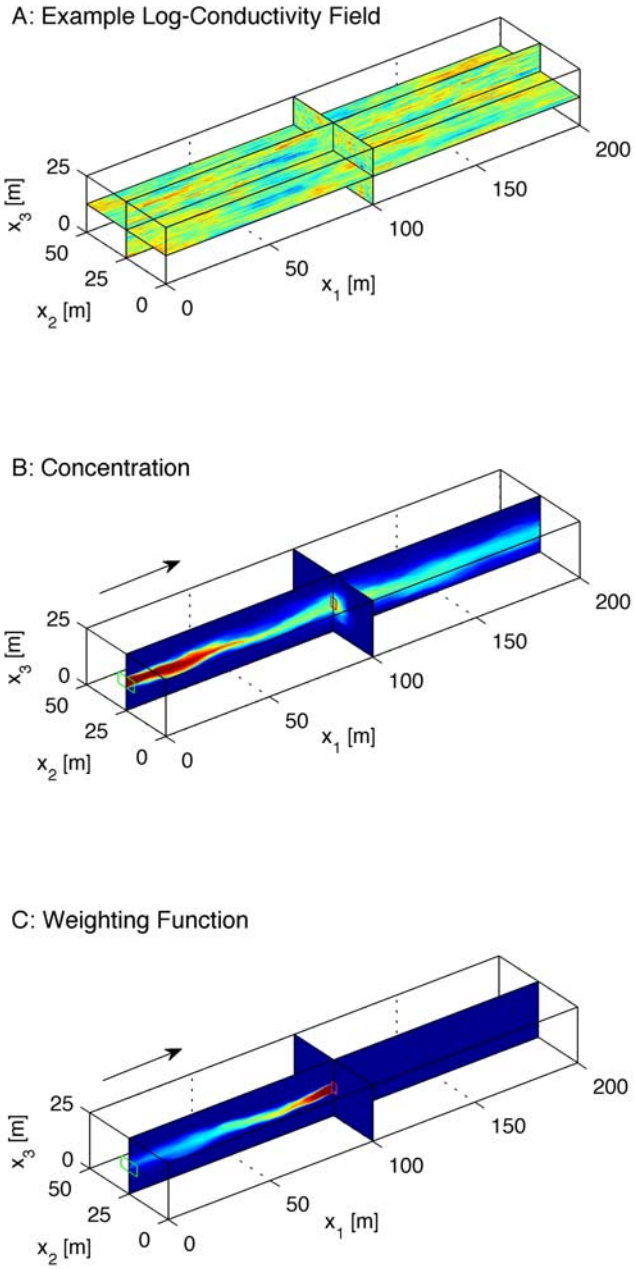

Figure 1. Example calculations of a forward and an adjoint transport problem. (a) Particular realization of the log conductivity field, (b) corresponding solution of the forward transport equation, and (c) solution of the adjoint transport equation. Green rectangle in Figures 1b and 1c indicates source area, and red rectangle indicates sampling area.

[18] The flux concentration (denoted by superscript "f") observed in the sampling area is given by the flux-weighted average concentration:

$$c^f_{\text{obs}} = \int_\Omega \frac{v_1(\boldsymbol{x})}{\bar{v}_1^{\chi}(\boldsymbol{x}^{obs})} \chi\left(\boldsymbol{x}_{2,3} - \boldsymbol{x}^{obs}_{2,3}\right) \times \delta\left(x_1 - x_1^{obs}\right) c(\boldsymbol{x}|c_{\text{in}}(\boldsymbol{x}'))\, \mathrm{d}\boldsymbol{x} \tag{10}$$

in which $\bar{v}_1^{\chi}(\boldsymbol{x}^{obs})$ is the mean longitudinal velocity in the sampling area:

$$\bar{v}_1^{\chi}\left(\boldsymbol{x}^{obs}\right) = \frac{\int_\Omega \chi\left(\boldsymbol{x}_{2,3} - \boldsymbol{x}^{obs}_{2,3}\right) \delta\left(x_1 - x_1^{obs}\right) v_1(\boldsymbol{x})\, \mathrm{d}\boldsymbol{x}}{\int_\Omega \chi\left(\boldsymbol{x}_{2,3} - \boldsymbol{x}^{obs}_{2,3}\right) \delta\left(x_1 - x_1^{obs}\right) \mathrm{d}\boldsymbol{x}} \tag{11}$$

The denominator of equation (11) is unity when the sampling function χ is chosen according to equation (9).

3.2. First-Order Semianalytical Approach to Estimate the Concentration pdf

3.2.1. Concept

[19] In order to compute the cumulative distribution function (cdf) of concentration averaged over a sampling area, we apply a conceptual framework similar to that of *Fiorotto and Caroni* [2002] and *Caroni and Fiorotto* [2005]. Rather than applying a forward model, in which an injected plume is tracked, we analyze where the solute measured in the sampling area is coming from. This is a so-called adjoint problem [e.g., *Neupauer and Wilson*, 1999]. For illustration, see Figure 1. In section 3.2.5, we briefly discuss why approximations made in the following are less restrictive in the adjoint framework than in the forward model. The velocity field in the adjoint problem is inverted, whereas the dispersion tensor remains the same. In transient cases, the time arrow would also be inverted. The adjoint steady state transport equations related to the measurements of the resident and flux concentrations, respectively (see equations (8) and (10)), differ in the source/sink term of the adjoint transport equation. The adjoint transport equation related to the flux concentration measurement is:

$$-\boldsymbol{v}\cdot\boldsymbol{\nabla}\psi - \boldsymbol{\nabla}\cdot(\boldsymbol{D}\boldsymbol{\nabla}\psi) = \chi\left(\boldsymbol{x}_{2,3} - \boldsymbol{x}^{obs}_{2,3}\right) \times \delta\left(x_1 - x_1^{obs}\right) v_1(\boldsymbol{x}) \text{ on } \Omega, \tag{12}$$

whereas the adjoint transport equation related to the resident concentration measurement is:

$$-\boldsymbol{v}\cdot\boldsymbol{\nabla}\psi - \boldsymbol{\nabla}\cdot(\boldsymbol{D}\boldsymbol{\nabla}\psi) = \chi\left(\boldsymbol{x}_{2,3} - \boldsymbol{x}^{obs}_{2,3}\right) \times \delta\left(x_1 - x_1^{obs}\right) \bar{v}_1^{\chi}\left(\boldsymbol{x}^{obs}\right) \text{ on } \Omega \tag{13}$$

Both adjoint transport equation, equations (12) and (13), are subject to the same boundary conditions:

$$\begin{aligned} \boldsymbol{n}\cdot(-\boldsymbol{v}\psi - \boldsymbol{D}\boldsymbol{\nabla}\psi) &= 0 \quad \text{on} \quad \Gamma_{\text{out}} \\ \boldsymbol{n}\cdot(\boldsymbol{D}\boldsymbol{\nabla}\psi) &= 0 \quad \text{on} \quad \Gamma_{\text{in}} \cup \Gamma_{\text{no}} \end{aligned} \tag{14}$$

[20] In the adjoint equations, the sampling area χ becomes an injection area, and the adjoint concentration ψ, denoted weighting function in the following, is advected backward and smeared by dispersion. The weighting function ψ has units of a cross-sectional density function. Neglecting for a moment minor modifications by local dispersion, the source-sink term in the adjoint equation for a measurement of the flux concentration, equation (12), leads to a distribution of ψ in the observation plane that is identical to the sampling function χ. In case of the adjoint equation for a resident concentration measurement, equation (13), by contrast, ψ fluctuates within the sampling

area. This is so because the left-hand side of equation (13) is dominated by the divergence of the advective flux, $\boldsymbol{v} \cdot \psi$. The normal component of the velocity $\boldsymbol{v}$ fluctuates within the sampling area. In case of the adjoint pde for a flux-weighted concentration measurement, equation (12), these fluctuations are balanced by a fluctuating right-hand side, whereas this is not the case in equation (13).

[21] The observed (flux or resident) concentration c_{obs} can now be computed by a weighted average of the inflow concentration c_{in} in the injection plane:

$$c_{\mathrm{obs}} = \int_{\Gamma_{\mathrm{in}}} \frac{v_1(\boldsymbol{x}')}{\bar{v}_1^{\chi}(\boldsymbol{x}^{obs})} \psi\left(\boldsymbol{x}'|\chi\left(\boldsymbol{x}^{obs}\right)\right) c_{\mathrm{in}}(\boldsymbol{x}')\, \mathrm{d}\boldsymbol{x}' \tag{15}$$

In analogy to equations (8) and (10), $\psi(\boldsymbol{x}'|\chi(\boldsymbol{x}^{obs}))$ expresses that the weighting function depends on the location and size of the sampling area. Equation (15) is an exact expression. In Appendix A, we briefly review the derivation of these equations by the continuous adjoint state method [*Sun and Yeh*, 1990].

[22] In the following, we assume that the cross term of the velocity ratio and ψc_{in} is negligible small. This implies that we can approximate equation (15) by:

$$c_{\mathrm{obs}} \approx \int_{\Gamma_{\mathrm{in}}} v_{rel} \psi\left(\boldsymbol{x}'|\chi\left(\boldsymbol{x}^{obs}\right)\right) c_{\mathrm{in}}(\boldsymbol{x}')\, \mathrm{d}\boldsymbol{x}' \tag{16}$$

in which v_{rel} is the ratio of the cross-sectional averaged velocity in the injection plane to that in the sampling area:

$$v_{rel} = \frac{\int_{\Gamma_{\mathrm{in}}} v_1(\boldsymbol{x}') \chi\left(\boldsymbol{x}'_{2,3} - \boldsymbol{x}^{obs}_{2,3}\right) \mathrm{d}\boldsymbol{x}'}{\bar{v}_1^{\chi}(\boldsymbol{x}^{obs})} \tag{17}$$

[23] In contrast to equation (15), the simplification by equation (16) leads to a uniform scaling factor caused by the ratio of velocities. Equation (17) implies that we compare the mean velocity in the sampling area to the mean velocity in the projection of the sampling area onto the injection plane. As will be shown in section 3.2.3, this approximation simplifies the statistics of v_{rel}.

[24] In the stochastic framework, the weighting function ψ and the relative velocity v_{rel} are random variables. Because of symmetry of the original and adjoint problems, the spatial moments of the local concentration c and the weighting function ψ behave statistically identically. Therefore, we can apply analytical results of first-order stochastic theory derived for the forward problem to compute the expected second central spatial moments in lateral directions of ψ in the injection plane as well as the expected value and covariance of first lateral spatial moments. The relative velocity v_{rel} acts as a correction factor accounting for plume expansion or contraction: A sampling area in a low-velocity region covers a lower density of streamlines than a sampling area of the same size in a region with about mean velocity. Likewise, a sampling area in a high-velocity region covers a higher density of streamlines. Therefore, sampling in a high-velocity (low-velocity) region requires a larger (smaller) influence area further upstream. In the following, we will assume that plume expansion/contraction is isotropic, that is, the entire spatial distribution of ψ in the injection area is scaled by $\sqrt{v_{rel}}$ in both lateral directions.

[25] Assuming a particular shape of $v_{rel}\psi$ for known first and second central moments results in a particular observed concentration c_{obs} according to equation (16). Assuming also a particular shape of the statistical distribution of first moments in the injection plane, we can compute the probability density of a certain combination of first moments. With these ingredients, we arrive at the following overall scheme, which will be discussed in detail in sections 3.2.2–3.2.4:

[26] 1. For given observation location $\boldsymbol{x}^{obs}$ and sampling function χ, compute the expected first and second central spatial moments and the covariance of first moments of the weighting function ψ in the injection plane. Compute also the variance of v_{rel} for given sampling function χ and distance between injection plane and sampling area.

[27] 2. Assuming a shape of the pdf, generate a set of first spatial moments of ψ and, independently, a set of v_{rel} values.

[28] 3. For each realization, scale the expected spatial second central moments of ψ in the injection plane by v_{rel}. Assuming a particular shape of the spatial distribution of $v_{rel}\psi$ in the injection plane and accounting for the first and second central spatial moments, compute for each realization the concentration c_{obs} in the sampling area according to equation (16).

[29] The scheme outlined above results in a set of c_{obs} values. With a sufficiently large number of realizations, we can compute the entire cumulative distribution function (cdf) of the concentration c_{obs} observed in the sampling area. Overall, rather than generating multiple realizations of the hydraulic conductivity field and performing flow-and-transport simulations using each of these realizations, we directly generate multiple realizations of expanded/contracted weighting functions $v_{rel}\psi$ in the injection plane. Because we rely on analytical expressions for the spatial moments and the shape of $v_{rel}\psi$, all computational steps can be performed rapidly (one million realizations within approximately 1 min CPU time on a standard PC).

3.2.2. Spatial Moments

[30] Effective dispersion quantifies the expected growth rate of second central spatial moments [*Kitanidis*, 1988]. In the initial value problem of transient transport, the difference of the expected value of second central spatial moments $\Delta\boldsymbol{\Xi}(t)$ to the spatial moments at time zero can be computed by [e.g., *Kitanidis*, 1988; *Dentz et al.*, 2000a, 2000b]:

$$\Delta\boldsymbol{\Xi}(t) = 2\int_0^t \boldsymbol{D}^e(\tau)\, \mathrm{d}\tau \tag{18}$$

with the effective dispersion tensor $\boldsymbol{D}^e$ which depends on the initial distribution. The change of second central spatial moments of the ensemble concentration $\Delta\boldsymbol{M}_{2c}(\mathrm{E}[c(t)])$ follows [e.g., *Gelhar and Axness*, 1983]:

$$\Delta\boldsymbol{M}_{2c}(\mathrm{E}[c(t)]) = 2\int_0^t \boldsymbol{D}^*(\tau)\, \mathrm{d}\tau \tag{19}$$

with the ensemble dispersion tensor $\boldsymbol{D}^*$. In a stationary velocity field, the expected value of the spatial first-moment vector $\boldsymbol{m}_1(t)$ is given by:

$$\mathrm{E}[\boldsymbol{m}_1(t)] = \bar{\boldsymbol{v}}t \tag{20}$$

with the arithmetic mean velocity vector $\bar{\boldsymbol{v}}$. The associated uncertainty is expressed by the covariance matrix $\boldsymbol{C}_{\boldsymbol{m}_1\boldsymbol{m}_1}(t)$ of first spatial moments:

$$\begin{aligned}\boldsymbol{C}_{\boldsymbol{m}_1\boldsymbol{m}_1}(t) &= \mathrm{E}[(\boldsymbol{m}_1(t) - \mathrm{E}[\boldsymbol{m}_1(t)]) \\ &\otimes (\boldsymbol{m}_1(t) - \mathrm{E}[\boldsymbol{m}_1(t)])] \\ &= \Delta\boldsymbol{M}_{2c}(\mathrm{E}[c(t)]) - \Delta\boldsymbol{\Xi}(t)\end{aligned} \tag{21}$$

[31] *Dentz et al.* [2000b] derived first-order expressions for $\boldsymbol{D}^*$ and $\boldsymbol{D}^e$ in second-order stationary velocity fields for arbitrary initial distributions $\chi(\boldsymbol{x})$:

$$\boldsymbol{D}^* = \boldsymbol{D} + \int_{V_y} \boldsymbol{S}_{\boldsymbol{v}'\boldsymbol{v}'^T}(\boldsymbol{y}) \times \frac{(d(\boldsymbol{y}) - a(\boldsymbol{y}))(1 - \exp(-(d(\boldsymbol{y}) + a(\boldsymbol{y}))t))}{d(\boldsymbol{y})^2 - a(\boldsymbol{y})^2}\,\mathrm{d}\boldsymbol{y} \tag{22}$$

$$\boldsymbol{D}^e = \boldsymbol{D}^* - \int_{V_y} (\tilde{\chi}(\boldsymbol{y}))^2 \boldsymbol{S}_{\boldsymbol{v}'\boldsymbol{v}'^T}(\boldsymbol{y})(d(\boldsymbol{y}) + a(\boldsymbol{y})) \times \frac{(\exp(-(d(\boldsymbol{y}) + a(\boldsymbol{y}))t) - \exp(-2d(\boldsymbol{y})t))}{d(\boldsymbol{y})^2 - a(\boldsymbol{y})^2}\,\mathrm{d}\boldsymbol{y} \tag{23}$$

in which $\boldsymbol{S}_{\boldsymbol{v}'\boldsymbol{v}'^T}$ is the power spectrum of the velocity fluctuations (for first-order approximations see *Gelhar and Axness* [1983]), $\boldsymbol{y}$ is the vector of frequencies, $\tilde{\chi}(\boldsymbol{y})$ is the Fourier transform of the initial distribution $\chi(\boldsymbol{x})$, and $a(\boldsymbol{y})$, $d(\boldsymbol{y})$ are given by

$$\begin{aligned}a(\boldsymbol{y}) &:= 2\pi\,\mathrm{i}\,\bar{\boldsymbol{v}}^T\boldsymbol{y} \\ d(\boldsymbol{y}) &:= 4\pi^2\boldsymbol{y}^T\boldsymbol{D}\boldsymbol{y}.\end{aligned} \tag{24}$$

[32] We assume that the initial distribution is centered about the origin. It is a rectangle $\chi(\boldsymbol{x}_{2,3})$ with dimensions w_2 and w_3 in directions x_2 and x_3 and a Dirac delta function in direction x_1. The corresponding Fourier transform $\tilde{\chi}(\boldsymbol{y})$ of the three-dimensional sampling function $\chi(\boldsymbol{x}_{2,3})\delta(x_1)$ is:

$$\tilde{\chi}(\boldsymbol{y}) = \mathrm{sinc}(w_2y_2)\mathrm{sinc}(w_3y_3)\ \forall\, y_1, \tag{25}$$

in which sinc(x) is the normalized sinc function defined as $\mathrm{sinc}(x) = \sin(\pi x)/\pi x$ and $\mathrm{sinc}(0) = 1$.

[33] Then, $\Delta\boldsymbol{\Xi}(t)$ and $\boldsymbol{C}_{\boldsymbol{m}_1\boldsymbol{m}_1}(t)$ can be computed by substituting equations (22), (23), and (25) into equations (18) and (19):

$$\boldsymbol{C}_{\boldsymbol{m}_1\boldsymbol{m}_1}(t) = 2\int_{V_y} (\mathrm{sinc}(w_2y_2))^2(\mathrm{sinc}(w_3y_3))^2 \times \boldsymbol{S}_{\boldsymbol{v}'\boldsymbol{v}'^T}(\boldsymbol{y})\left[\frac{1 - \exp(-(d(\boldsymbol{y}) + a(\boldsymbol{y}))t)}{d(\boldsymbol{y})^2 - a(\boldsymbol{y})^2} + \frac{(d(\boldsymbol{y}) + a(\boldsymbol{y}))(\exp(-2d(\boldsymbol{y})t) - 1)}{2d(\boldsymbol{y})\left(d(\boldsymbol{y})^2 - a(\boldsymbol{y})^2\right)}\right]\mathrm{d}\boldsymbol{y} \tag{26}$$

and

$$\Delta\boldsymbol{\Xi}(t) = 2\left[\boldsymbol{D}t + \int_{V_y} \boldsymbol{S}_{\boldsymbol{v}'\boldsymbol{v}'^T}(\boldsymbol{y})(d(\boldsymbol{y}) - a(\boldsymbol{y}))^2 \times \left[\frac{(d(\boldsymbol{y}) + (a(\boldsymbol{y}))t + \exp(-(d(\boldsymbol{y}) + a(\boldsymbol{y}))t) - 1)}{\left(a(\boldsymbol{y})^2 - a(\boldsymbol{y})^2\right)^2} - (\mathrm{sinc}(w_2y_2))^2(\mathrm{sinc}(w_3y_3))^2 \times \left[\frac{1 - \exp(-(d(\boldsymbol{y}) + a(\boldsymbol{y}))t)}{d(\boldsymbol{y})^2 - a(\boldsymbol{y})^2} + \frac{(d(\boldsymbol{y}) + a(\boldsymbol{y}))(\exp(-2d(\boldsymbol{y})t) - 1)}{2d(\boldsymbol{y})\left(d(\boldsymbol{y})^2 - a(\boldsymbol{y})^2\right)}\mathrm{d}\boldsymbol{y}\right]\right]\right]. \tag{27}$$

[34] These expressions are for transient transport of a solute with a particular initial distribution. In steady state transport, we are only interested in the spatial moments in transverse directions as function of the longitudinal coordinate x_1, which we evaluate from the above expressions at the mean travel time $t = x_1/\bar{v}$. In our implementation, we evaluate equations (26) and (27) in the Fourier space associated to an extended periodic spatial domain. Fourier transformations are performed by the Fast Fourier Transformation (FFT) implemented in Matlab.

3.2.3. Estimating the Distribution of Relative Velocity

[35] In our framework, the relative velocity v_{rel}, appearing in equation (16), acts as a correction factor to account for expansion or contraction of the plume cross section. As already discussed in section 3.2.1, we compare the mean velocity in the sampling area to the mean velocity in the projection of the sampling area onto the injection plane. In principle, it would be possible to account for the lateral displacement of ψ in the injection plane and its expansion due to transverse effective dispersion.

[36] In a second-order stationary velocity field, we can compute the variance of v_{rel} using first order theory by:

$$\sigma^2_{v_{rel}} = \frac{2}{\bar{v}_1^2}\left(R_{v_1v_1}(\boldsymbol{0}) - R_{v_1v_1}\left(\boldsymbol{x}^{obs} - \boldsymbol{x}'\right)\right), \tag{28}$$

in which $R_{v_1v_1}(\boldsymbol{h})$ is the autocovariance function of the longitudinal velocity component with distance vector $\boldsymbol{h}$. In the given framework, $\boldsymbol{h}$ equals $[x_1^{obs}, 0, 0]$. For mean flow in direction x_1, the scaled covariance function $R_{v_1v_1}(\boldsymbol{h})/\bar{v}_1^2$ of the filtered longitudinal velocity component can be estimated in first order by [e.g., *Gelhar and Axness*, 1983]:

$$\frac{R_{v_1v_1}(\boldsymbol{h})}{\bar{v}_1^2} = \int_{\infty} \tilde{\chi}(\boldsymbol{y})^2\left(1 - \frac{y_1^2}{\boldsymbol{y}\cdot\boldsymbol{y}}\right)^2 S_{Y'Y'}(\boldsymbol{y})\exp(2\pi i\boldsymbol{h}\cdot\boldsymbol{y})\,d\boldsymbol{y} \tag{29}$$

[37] We model v_{rel} as random lognormally distributed variable [see *Nowak et al.*, 2008] with unit geometric mean (implying that the statistics of v_{rel} are identical to those of v_{rel}^{-1}) and arithmetic variance σ^2_{vrel}. Thus the cdf of v_{rel} is:

$$F_{v_{rel}}(v_{rel}) = \frac{1}{2} + \frac{1}{2}\mathrm{erf}\left(\frac{\ln(v_{rel})}{\sqrt{2\ln\left(\frac{1}{2} + \sqrt{\frac{1}{4} + \sigma^2_{v_{rel}}}\right)}}\right) \tag{30}$$

3.2.4. Computing the cdf of Concentration

[38] In the first step, we transfer the expressions for lateral moments presented in section 3.2.2 to our adjoint transport problem (see equation (12)). We consider a rectangular observation area centered about the point $\boldsymbol{x}^{obs}$. The widths of the rectangle are w_2 and w_3 in the horizontal and vertical transverse coordinate, respectively. The inflow boundary is at $x_1 = 0$. We denote the first transverse moments of the weighting function ψ in the injection plane by $\boldsymbol{\xi}_{2,3}$. The expected value of $\boldsymbol{\xi}_{2,3}$ equals the transverse coordinates $\boldsymbol{x}^{obs}_{2,3}$ of the observation point, whereas the covariance matrix $\boldsymbol{C}_{\boldsymbol{\xi}\boldsymbol{\xi};2,3}$ equals $\boldsymbol{C}_{\boldsymbol{m}_1\boldsymbol{m}_1;2,3}\ (x_1^{obs}/\bar{v})$ as computed by equation (26). The expected second central transverse moments $\Delta\boldsymbol{\Xi}_{2,3}$ of the weighting function ψ are given by equation (27). This covariance matrix depends on the travel distance, x_1^{obs}, the mean velocity, $\bar{v}$, the local dispersion tensor, $\boldsymbol{D}$, and the size of the observation rectangle, (w_2, w_3).

[39] In the second step, we consider the ensemble of weighting functions ψ (0, x'_2, x'_3) in the injection plane. First-order analysis does not give the uncertainty of second central spatial moments, but we consider the additional random scaling factor v_{rel} which produces variability of second central spatial moments of $v_{rel}\psi$. For a point-like observation, we assume a Gaussian spatial distribution in the injection plane of $v_{rel}\psi^p\ (\boldsymbol{x}'_{2,3}|\boldsymbol{\xi}_{2,3})$ (superscript "p" denotes point-like measurements) centered about the first moments $\boldsymbol{\xi}_{2,3}$ (which are assumed to be given in this step) with covariance matrix $\Delta\boldsymbol{\Xi}_{2,3}\ (x_1^{obs}/\bar{v})/v_{rel}$:

$$v_{rel}\psi^p\left(\boldsymbol{x}'_{2,3}|\boldsymbol{\xi}_{2,3}\right) = \frac{v_{rel}}{2\pi\sqrt{\Delta\Xi_{22}\Delta\Xi_{33}}} \times \exp\left(-\frac{1}{2}\left(\sum_{i=2}^{3}\frac{\left(x'_i-\xi_i\right)^2}{\Delta\Xi_{ii}/v_{rel}}\right)\right), \tag{31}$$

in which we have dropped the argument ${x^{obs}}_1/\bar{v}$ of $\Delta\boldsymbol{\Xi}_{2,3}$ and made use of the fact that this matrix has zero off-diagonal entries.

[40] For a rectangular sampling area with widths w_2 and w_3, the corresponding weighting function times the correction factor $v_{rel}\psi^{SV}(\boldsymbol{x}'_{2,3}|\boldsymbol{\xi}_{2,3})$ (superscript "SV" denotes measurements over a larger sampling area) is an integrated Gaussian distribution:

$$v_{rel}\psi^{SV}\left(\boldsymbol{x}'_{2,3}|\boldsymbol{\xi}_{2,3}\right) = \frac{v_{rel}}{4w_2w_3}\times\prod_{i=2}^{3}\left[\mathrm{erf}\left(\frac{\xi_i-\frac{1}{2\sqrt{v_{rel}}}w_i-x'_i}{\sqrt{2\Delta\Xi_{ii}/v_{rel}}}\right) - \mathrm{erf}\left(\frac{\xi_i+\frac{1}{2\sqrt{v_{rel}}}w_i-x'_i}{\sqrt{2\Delta\Xi_{ii}/v_{rel}}}\right)\right] \tag{32}$$

Both expressions depend on the sampling area via $\Delta\boldsymbol{\Xi}_{2,3}$.

[41] In the third step, we consider the concentration in the inflow $c_{in}(\boldsymbol{x}')$. For simplicity of the further derivations, we set $c_{in}(\boldsymbol{x}')$ to unity within a rectangle of size $L_2 \times L_3$ centered about the origin, and zero outside. Substituting the weighting function times the relative velocity $v_{rel}\psi^p(\boldsymbol{x}'_{2,3}|\boldsymbol{\xi}_{2,3})$ and $v_{rel}\psi^{SV}(\boldsymbol{x}'_{2,3}|\boldsymbol{\xi}_{2,3})$ into equation (16) and considering equation (17) yields the observed concentration $c_{\mathrm{obs}}(\boldsymbol{\xi}_{2,3},\ v_{rel})$ for given vector of first moments $\boldsymbol{\xi}_{2,3}$ of the weighting function ψ in the injection plane and relative velocity v_{rel}, namely, for point-like observations:

$$\begin{aligned} c^p_{\mathrm{obs}}\left(\boldsymbol{\xi}_{2,3}, v_{rel}\right) &= \int_{-L_2/2}^{+L_2/2}\int_{-L_3/2}^{+L_3/2} v_{rel}\psi^p\left(\boldsymbol{x}'_{2,3}|\boldsymbol{\xi}_{2,3}\right)\mathrm{d}x'_3\ \mathrm{d}x'_2 \\ &= \frac{1}{4}\prod_{i=2}^{3}\left(\mathrm{erf}\left(\frac{-\frac{1}{2}L_i-\xi_i}{\sqrt{2\Delta\Xi_{ii}/v_{rel}}}\right) - \mathrm{erf}\left(\frac{+\frac{1}{2}L_i-\xi_i}{\sqrt{2\Delta\Xi_{ii}/v_{rel}}}\right)\right) \end{aligned} \tag{33}$$

and for observations over a rectangle:

$$\begin{aligned} c^{SV}_{\mathrm{obs}}\left(\boldsymbol{\xi}_{2,3}, v_{rel}\right) &= \int_{-L_2/2}^{+L_2/2}\int_{-L_3/2}^{+L_3/2} v_{rel}\psi^{SV}\left(\boldsymbol{x}'_{2,3}|\boldsymbol{\xi}_{2,3}\right)\mathrm{d}x'_3\ \mathrm{d}x'_2 \\ &= \frac{v_{rel}}{4w_2w_3}\prod_{i=2}^{3}\left[\left(\left(\left(+\frac{1}{2}L_i+\frac{1}{2\sqrt{v_{rel}}}w_i-\xi_i\right)\right.\right.\right. \\ &\quad\times\mathrm{erf}\left(\frac{+\frac{1}{2}L_i+\frac{1}{2\sqrt{v_{rel}}}w_i-\xi_i}{\sqrt{2\Delta\Xi_{ii}/v_{rel}}}\right) \\ &\quad\left.+\sqrt{\frac{2\Delta\Xi_{ii}}{\pi v_{rel}}}\exp\left(\frac{+\frac{1}{2}L_i+\frac{1}{2\sqrt{v_{rel}}}w_i-\xi_i}{2\Delta\Xi_{ii}/v_{rel}}\right)\right) \\ &\quad-\left(\left(+\frac{1}{2}L_i-\frac{1}{2\sqrt{v_{rel}}}w_i-\xi_i\right)\right. \\ &\quad\times\mathrm{erf}\left(\frac{+\frac{1}{2}L_i-\frac{1}{2\sqrt{v_{rel}}}w_i-\xi_i}{\sqrt{2\Delta\Xi_{ii}/v_{rel}}}\right) \\ &\quad\left.\left.+\sqrt{\frac{2\Delta\Xi_{ii}}{\pi v_{rel}}}\exp\left(\frac{+\frac{1}{2}L_i-\frac{1}{2\sqrt{v_{rel}}}w_i-\xi_i}{2\Delta\Xi_{ii}/v_{rel}}\right)\right)\right) \\ &\quad-\left(\left(\left(-\frac{1}{2}L_i+\frac{1}{2\sqrt{v_{rel}}}w_i-\xi_i\right)\right.\right. \\ &\quad\times\mathrm{erf}\left(\frac{-\frac{1}{2}L_i+\frac{1}{2\sqrt{v_{rel}}}w_i-\xi_i}{\sqrt{2\Delta\Xi_{ii}/v_{rel}}}\right) \\ &\quad\left.+\sqrt{\frac{2\Delta\Xi_{ii}}{\pi v_{rel}}}\exp\left(\frac{-\frac{1}{2}L_i+\frac{1}{2\sqrt{v_{rel}}}w_i-\xi_i}{2\Delta\Xi_{ii}/v_{rel}}\right)\right) \\ &\quad-\left(\left(-\frac{1}{2}L_i-\frac{1}{2\sqrt{v_{rel}}}w_i-\xi_i\right)\right. \\ &\quad\times\mathrm{erf}\left(\frac{-\frac{1}{2}L_i-\frac{1}{2\sqrt{v_{rel}}}w_i-\xi_i}{\sqrt{2\Delta\Xi_{ii}/v_{rel}}}\right) \\ &\quad\left.\left.\left.+\sqrt{\frac{2\Delta\Xi_{ii}}{\pi v_{rel}}}\exp\left(\frac{-\frac{1}{2}L_i-\frac{1}{2\sqrt{v_{rel}}}w_i-\xi_i}{2\Delta\Xi_{ii}/v_{rel}}\right)\right)\right)\right)\right] \end{aligned} \tag{34}$$

[42] In the given framework, the observed concentration according to equations (33) and (34) depends on the vector of first moments $\boldsymbol{\xi}_{2,3}$ and on the relative velocity v_{rel}. The joint probability of $\boldsymbol{\xi}_{2,3}$ and v_{rel} can thus be mapped to the probability of c_{obs}.

[43] We assume that the statistical distribution $F_{m_1}(\boldsymbol{\xi}_{2,3})$ of the first-moment vector $\boldsymbol{\xi}_{2,3}$ is Gaussian:

$$F_{m_1}\left(\boldsymbol{\xi}_{2,3}\right) \sim \mathcal{N}\left(\boldsymbol{x}^{obs}_{2,3}, \boldsymbol{C}_{\boldsymbol{m}_1\boldsymbol{m}_1;2,3}\left(\frac{x_1^{obs}}{\bar{v}}\right)\right). \tag{35}$$

[44] For the concentration observed in the sampling area around the observation point $\boldsymbol{x}^{obs}$, we generate a set of 8 ·

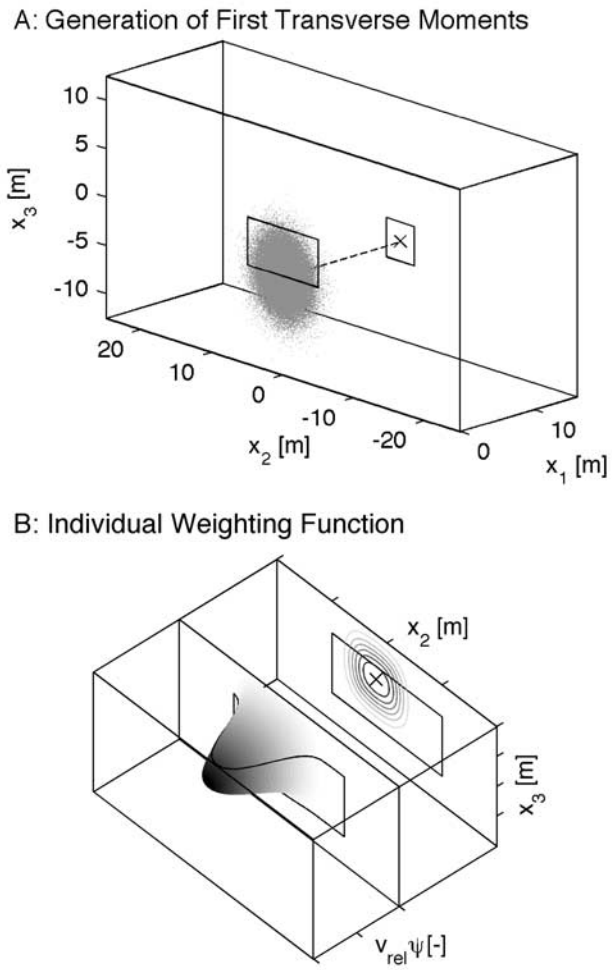

Figure 2. Illustration of the semianalytical approach for calculating the concentration cdf. (a) Large rectangle in the front indicates solute source, cross indicates observation point, small rectangle in the back indicates sampling area, gray dots indicate realizations of first transverse moments as given in equation (35), and dashed line indicates projection of the observation point onto the inflow plane. (b) Weighting function $v_{rel}\psi$ in the injection plane according to equation (32) for a particular realization of first transverse moments with projection of the source area onto $v_{rel}\psi$ (white line); rear layer indicates inflow plane with boundary of source area and contour lines of $v_{rel}\psi$.

10^6 realizations of $\boldsymbol{\xi}_{2,3}$ drawn from the distribution $F_{m_1}(\boldsymbol{\xi}_{2,3})$ according to equation (35) and a set of v_{rel} values drawn from the lognormal distribution given in equation (30). For illustration of the $\boldsymbol{\xi}_{2,3}$ values see Figure 2a. For each realization, we compute $c_{\text{obs}}(\boldsymbol{\xi}_{2,3}, v_{rel})$ according to equations (33) and (34), which may be visualized by Figure 2b. From the set of realizations, we compute the empirical cumulative distribution function $\widehat{F}_c^{ana}(c_{\text{obs}}^{\text{tar}})$ for a given target concentration $c_{\text{obs}}^{\text{tar}}$ by:

$$\widehat{F}_c^{ana}\left(c_{\text{obs}}^{\text{tar}}\right) = \frac{\text{number of realizations with } c_{\text{obs}} \le c_{\text{obs}}^{\text{tar}}}{\text{total number of realizations}} \qquad (36)$$

[45] With the outlined semianalytical approach, the concentration cdf can be computed quite rapidly for given observation location, sampling volume, local dispersion tensor, mean velocity, and statistical parameters of the log-conductivity field.

3.2.5. Discussion of the Approach

[46] In the approach presented by *Fiorotto and Caroni* [2002] and *Caroni and Fiorotto* [2005], considering an extended sampling volume requires the integration of the two-particle covariance function of displacement over all combinations of two points within the sampling area, which is cumbersome. The latter authors also did not consider the expansion/contraction factor v_{rel}. Given the first spatial moments of displacement, the scaled weighting function $v_{rel}\psi^{SV}(\boldsymbol{x}'_{2,3}|\boldsymbol{\xi}_{2,3})$, computed in our approach, equals the probability density that a particle found anywhere within the sampling area originates from a particular point $\boldsymbol{x}'$ in the injection plane.

[47] The approach outlined above depends on a number of assumptions that may be questioned. First, the amount of lateral smearing, expressed by $\Delta\Xi_{2,3}/v_{rel}$, is set to the expected value of second central spatial moments divided by the correction factor. Numerical experiments, however, indicate that mixing shows strong spatial fluctuations [e.g., *Cirpka and Kitanidis*, 2000], which might not be totally covered by our approach [see also *Werth et al.*, 2006]. Using first-order stochastic theory, it is difficult to quantify the uncertainty of $\Delta\Xi_{2,3}$ [e.g., *Eberhard*, 2004]. The correction factor v_{rel} accounts only for a single mechanism (expansion and contraction of plumes) causing uncertainty of $\Delta\Xi_{2,3}$. Second, we calculate the dispersion tensor only to first order accuracy. *Dentz et al.* [2002] and *Attinger et al.* [2004] showed that especially for large log-conductivity variances this might be insufficient. Third, we assume a Gaussian shape of the weighting function in the injection plane, whereas in reality the weighting function for a given realization of the log-conductivity field will have a more irregular shape. The difference between the irregular shape and the assumed Gaussian shape grows with the size of the injection source. In the adjoint equations, the sampling area and the injection source are interchanged. Thus, whenever the sampling area is smaller than the injection source, the adjoint approach will be less biased than a formulation based on the forward equations. Furthermore we believe that the assuming a particular adjoint plume shape is less restrictive than the other two simplifications mentioned above, because the exact shape of $v_{rel}\psi(\boldsymbol{x}'_{2,3}|\boldsymbol{\xi}_{2,3})$ is not too relevant. The important quantity is the integral of $v_{rel}\psi(\boldsymbol{x}'_{2,3}|\boldsymbol{\xi}_{2,3})$ over the injection area (see equations (33) and (34)).

3.3. Monte Carlo Simulation Using Realizations of Log-Conductivity Fields: Numerical Methods

[48] For comparison purpose, we perform numerical Monte Carlo simulations of flow and transport using multiple random realizations of the log-conductivity field. The $\ln(K)$ fields are generated by the spectral approach of *Dietrich and Newsam* [1993]. Flow and transport are simulated by the Finite Element Method (FEM) using trilinear base functions on a structured, orthogonal grid. The conductivity is defined element by element. For the stabilization of transport, we use the streamline upwind Petrov Galerkin (SUPG) method of *Brooks and Hughes*

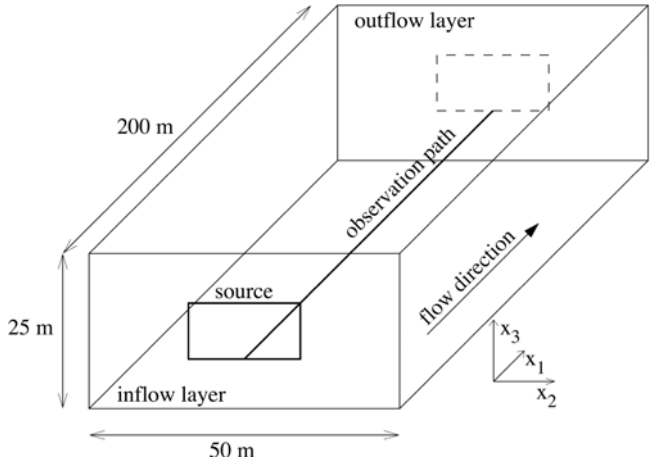

Figure 3. Setting of the computational domain and location of the observation path. The injection source is 10 m × 5 m (does not fit to the scale).

[1982] with slightly enhanced streamline diffusion if necessary. The resulting systems of linear equations are solved by a (bi)conjugate gradient method with algebraic multigrid preconditioning [*Stüben*, 2001]. The sampling of concentration is simulated by taking an arithmetic average of concentration in the sampling area (resident concentration, see equation (8)). While resident and flux concentrations are known to differ considerably in transient transport (namely, in the time of breakthrough), we assume that these differences are much less pronounced under conditions of steady state transport. In order to obtain a good empirical approximation of the concentration pdf, we found no less than 10,000 realizations to be sufficient. The empirical cumulative distribution function $\widehat{F}_c^{num}(c_{\text{obs}}^{\text{tar}})$ for a given target concentration $c_{\text{obs}}^{\text{tar}}$ is computed by:

$$\widehat{F}_c^{num}\left(c_{\text{obs}}^{\text{tar}}\right) = \frac{\text{number of realizations with } c_{\text{sim}} \le c_{\text{obs}}^{\text{tar}}}{\text{total number of realizations}} \tag{37}$$

in which c_{sim} is the simulated concentration averaged over a given sampling area in a single realization. Likewise the empirical pdf $\widehat{f}_h(c)$ is given by a histogram, that is, the number of realizations falling into a defined range centered about c, divided by the total number of realizations and the step size h.

3.4. Fitting of Parametric Distributions

[49] We hypothesize that the semianalytical and empirical distributions of steady state concentration can be described sufficiently well by two-parametric statistical distributions. Consequently, a data fitting procedure is needed. Some parametric distributions, such as the Gaussian one, are unbounded. Concentration, however, ranges between zero and one, if normalized by the inflow concentration. In the fitting procedure, it is mandatory to penalize the fractions of the parametric distributions that are outside of the physically possible range. For this purpose, we extend the least-square fitting procedure such that probability mass outside the unit interval is considered in the goodness of the fitting curve. The resulting extended error norm for the distance between a stepwise constant empirical (or semianalytical) pdf $\widehat{f}_h(c)$ within the unit domain and a continuous parametric pdf f is:

$$\varepsilon^2\left(\widehat{f}_h, f\right) = \sum_{i=1}^{m} h_i\left(\widehat{f}_h(c_i) - f(c_i)\right)^2 + \int_{-\infty}^{0} f^2(x)\,\mathrm{d}x + \int_{1}^{\infty} f^2(x)\,\mathrm{d}x, \tag{38}$$

in which the latter two terms penalize the sections of f falling outside the unit domain.

[50] We fit the empirical results to two parametric distributions: the Gaussian distribution and the beta distribution given by:

$$f_{\mathcal{B}(\alpha,\beta)}(x) = \begin{cases} \dfrac{\Gamma(\alpha+\beta)}{\Gamma(\alpha)\Gamma(\beta)} x^{\alpha-1}(1-x)^{\beta-1} & \forall x \in [0,1] \\ 0 & \text{otherwise} \end{cases} \tag{39}$$

in which $\Gamma(z) = \int_0^\infty t^{z-1}\exp(-t)\,\mathrm{d}t$ denotes the well-known Gamma function and α, $\beta > 0$ are the nonnegative parameters of the beta distribution. The beta distribution was already used by *Fiorotto and Caroni* [2002], *Caroni and Fiorotto* [2005], and *Bellin and Tonina* [2007].

[51] We perform the fitting of parametric distributions to the concentration pdf's of both the semianalytical and the numerical Monte Carlo methods.

4. Application to a Hypothetical Test Problem

4.1. Description of the Test Problem

[52] We consider an orthogonal domain of the size 200 m × 50 m × 25 m. For the generation of conductivity fields we assume an exponential model of the covariance function (see equation (7)), characterized by the variance σ_Y^2 and the vector of correlation lengths $\boldsymbol{\lambda} = [\lambda_1, \lambda_2, \lambda_3]$:

$$R_{Y',Y'}(|\boldsymbol{x}-\boldsymbol{z}|) = \sigma_Y^2 \exp\left(-\sqrt{\sum_{i=1}^{3}\left(\frac{x_i - z_i}{\lambda_i}\right)^2}\right). \tag{40}$$

[53] Flow is in direction x_1 with mean velocity $\bar{v} = 1.157 \cdot 10^{-5}$ m/s(=1 *m/d*). The size of the rectangular injection area is 10 m × 5 m. As illustrated in Figure 3, we consider a path of observation points oriented in x_1 direction. The path starts at the center of the bottom edge of the plume. The vector of correlation lengths is $\boldsymbol{\lambda} = [10, 5, 2.5]$ [m], and the variance σ_Y^2 of $\ln(K)$ is unity unless otherwise noted. The transport parameters are chosen for two test cases differing in their transverse Péclet numbers:

$$\mathrm{Pe}_i = \frac{\bar{v}\lambda_i}{D_i} \tag{41}$$

[54] In test case 1, $\mathrm{Pe}_2 = 250$ and $\mathrm{Pe}_3 = 125$, whereas in test case 2 the values are $\mathrm{Pe}_2 = 25{,}000$ and $\mathrm{Pe}_3 = 12{,}500$. The resolution of the FEM grid is 2 m in the longitudinal direction and 1/3 m in both transverse directions. The FEM grid has $\sim 1.1 \cdot 10^6$ nodes.

4.2. Individual Results of Both Methods

[55] Using the semianalytical method described in section 3.2 to evaluate the cdf of concentration, we

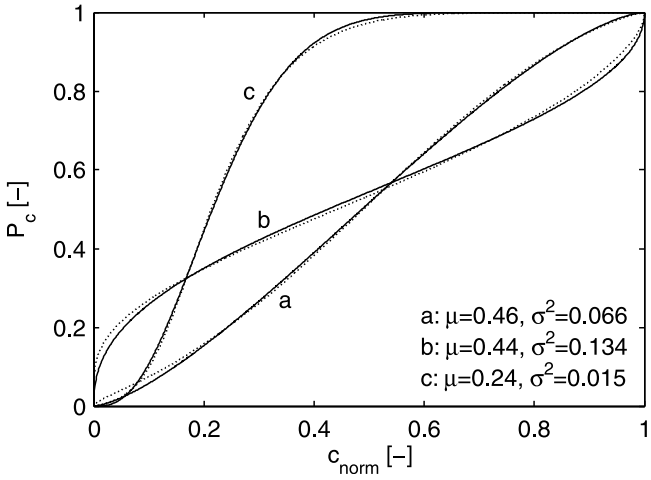

Figure 4. Cumulative distribution function (cdf) of concentration in the semianalytical approach. Dashed line indicates semianalytical cdf, and solid line indicates fitted beta distribution. Line a indicates travel distance $x_1 = \lambda_1$ and sampling volume 4 m × 4 m, line b indicates travel distance $x_1 = 2\lambda_1$ for a point measurement, and line c indicates $x_1 = 16\lambda_1$ for sampling volume 8 m × 8 m.

obtain a reasonable match when fitting beta distributions to the results. Figure 4 shows generated (dotted line) and fitted (solid line) cdf's for selected points along the observation path and for selected sampling sizes. The difference between the two curves is small. The biggest difference is observed for relatively small travel distances at small concentration values.

[56] Figure 5 shows the impact of increasing the sampling volume on the concentration pdf at two points along the observation path. Enlarging the sampling volume changes the shape of the distribution. For point-like observations at short travel distance, the concentration pdf is bimodal, reflecting pseudobinary behavior (the observation points lies either within the plume or outside). Slightly enlarging the sampling volume leads to a multimodal pdf with an additional peak at intermediate concentrations. Considering very large sampling volumes, finally, the pdf becomes unimodal with a single peak at intermediate concentrations. Figure 6 shows the effect of travel distance on the concentration pdf for both point-like observations and sampling over a large sampling area. Increasing the travel distance has a similar effect on the shape of the concentration pdf as increasing the sampling volume. The point from which onward the beta fitted concentration pdf is unimodal, is at 43 m for the point-like measurements, at 35 m for a sampling area of 2 m × 2 m, and for sampling areas larger than 3.33 m × 3.33 m the shape of the beta fitted pdf's is unimodal within the complete domain.

[57] Figures 7–9 show the results of our Monte Carlo simulations. Figures 7 and 8 show the empirical pdf's of concentration as function of travel distance. The plots differ in the transverse Péclet numbers and the size of the sampling area. The numerical results confirm the transition from a bimodal to a unimodal distribution for increasing travel distance, transverse dispersion, or sampling volume. The point from which onward the beta fitted concentration pdf is unimodal, is at 36 m for the point-like measurements and for sampling areas larger than 1 m × 1 m the shape of the beta fitted pdf's is unimodal within the complete domain. Figure 9 shows plots of the fitting error ε according to equation (38) for the numerical Monte Carlo simulation. With increasing distance to the solute source we observe, that the concentration pdf obtained from the numerical Monte Carlo simulations can also be fitted by a Gaussian pdf. From a certain distance on, the error norms of the beta and Gaussian fits are in the same range. Increasing the sampling volume decreases the distance to the contaminant source for which a (quasi-)Gaussian distribution is not yet observed. In the numerical Monte Carlo simulations the multimodal shape of the concentration pdf (three probability peaks, two at the extreme values and one at an intermediate concentration) can be observed only in a narrow range of travel distance. The probability peaks are also not as distinct as in the semianalytical results.

[58] All results shown so far refer to the observation points along a path starting at the center of the bottom edge

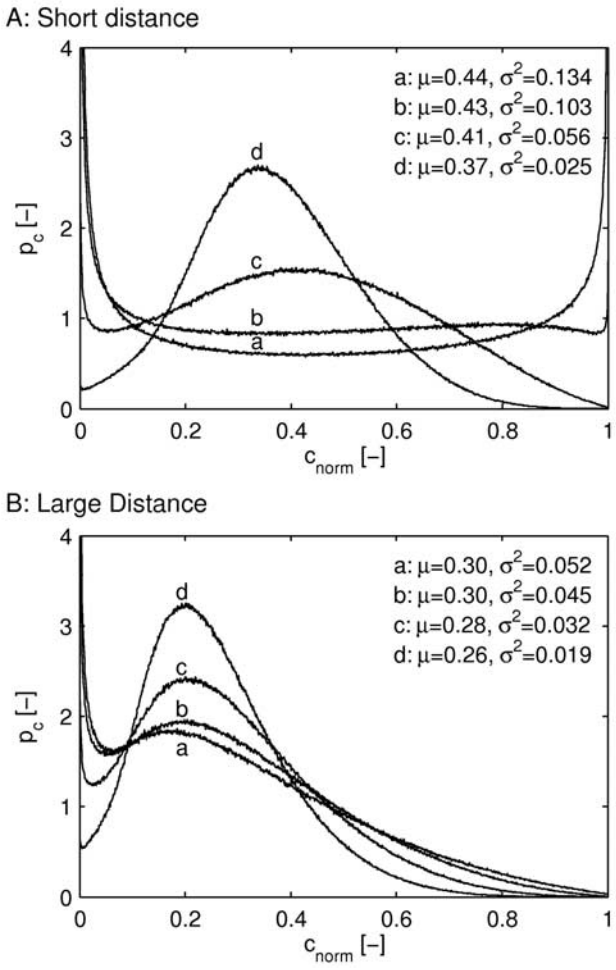

Figure 5. Development of the semianalytical concentration pdf along the observation path with increasing sampling volume. Line a indicates point-like observation, line b indicates observation over 2.67 m × 2.67 m, line c indicates observation over 5.33 m × 5.33 m, and line d indicates observation over 8 m × 8 m. (a) Distance $x_1^{obs} = 2\lambda_1$ and (b) distance $x_1^{obs} = 10\lambda_1$.

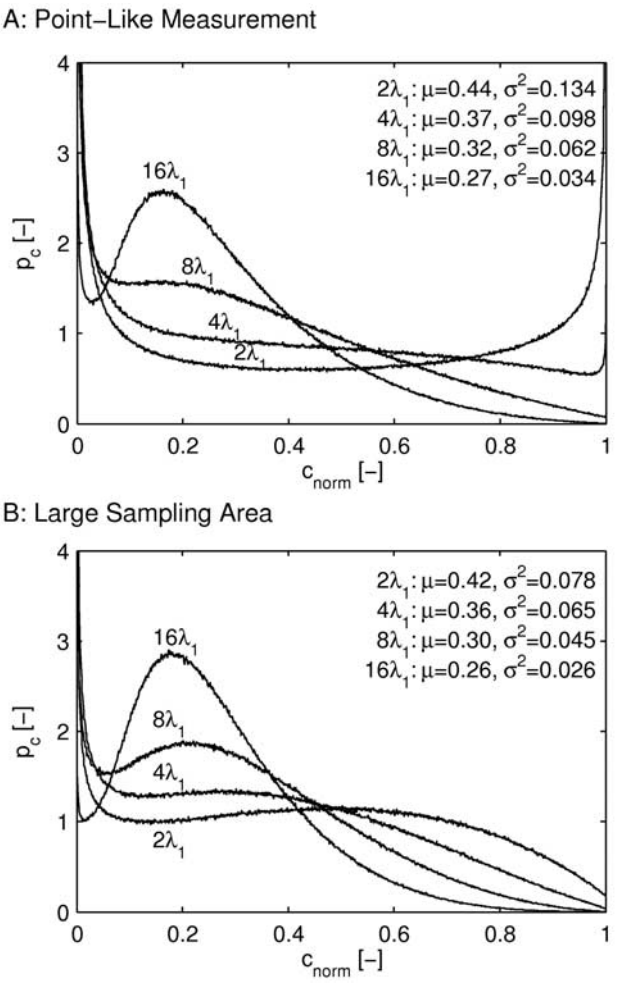

Figure 6. Development of the semianalytical concentration pdf along the observation path with increasing distance to the contaminant source (see labels). (a) Point-like measurement and (b) sampling area 4 m × 4 m.

of the plume. We have also considered other observation paths starting at other edges of the plume and in the plume center. These results are not shown explicitly. As may be expected, the observed pdf following the center line of the plume did not show the bimodal shape. The observation paths along different edges of the plume are qualitatively similar to the discussed observation path. Furthermore, we performed numerical Monte Carlo simulations for different values of log conductivity variance, namely, $\sigma_Y^2 = 0.05$, $\sigma_Y^2 = 1/3$, and $\sigma_Y^2 = 3$. Here we observed that increasing the variance leads to a faster transition from a bimodal concentration pdf to a quasi-Gaussian one. We are careful in overinterpreting these findings because numerical artifacts, such as numerical dispersion and oscillations, may have affected the results.

4.3. Comparison of the Methods

[59] For comparison of the semianalytical and numerical approaches, we use the settings described in section 4.1. The log-conductivity variance is set to either $\sigma_Y^2 = 0.05$ or $\sigma_Y^2 = 1$ and the numerical results with small Péclet numbers, namely, $Pe_2 = 250$ and $Pe_3 = 125$, are used.

[60] For comparison of the statistical distributions obtained by the semianalytical and numerical approaches, we use the same error norm ε as used in the evaluation of fitting parametric distributions, namely, the root-mean-square error as defined in equation (38). Figure 10 shows ε as a function of distance x_1 from the injection plane for $\sigma_Y^2 = 0.05$ and $\sigma_Y^2 = 1$. Quite obviously, decreasing the variance of log-conductivity also decreases the mean square error ε between the statistical distributions obtained by the semianalytical and the numerical approaches. We conjecture that the two statistical distributions become identical at the small-variance limit.

[61] In Figure 11 the pdf's of the semianalytical (black line) and the numerical (gray line) approaches are shown for different travel distances along the observation path. Figure 11a shows the results for point-like measurements, Figure 11b for a medium-sized sampling area, and Figure 11c for a large sampling area.

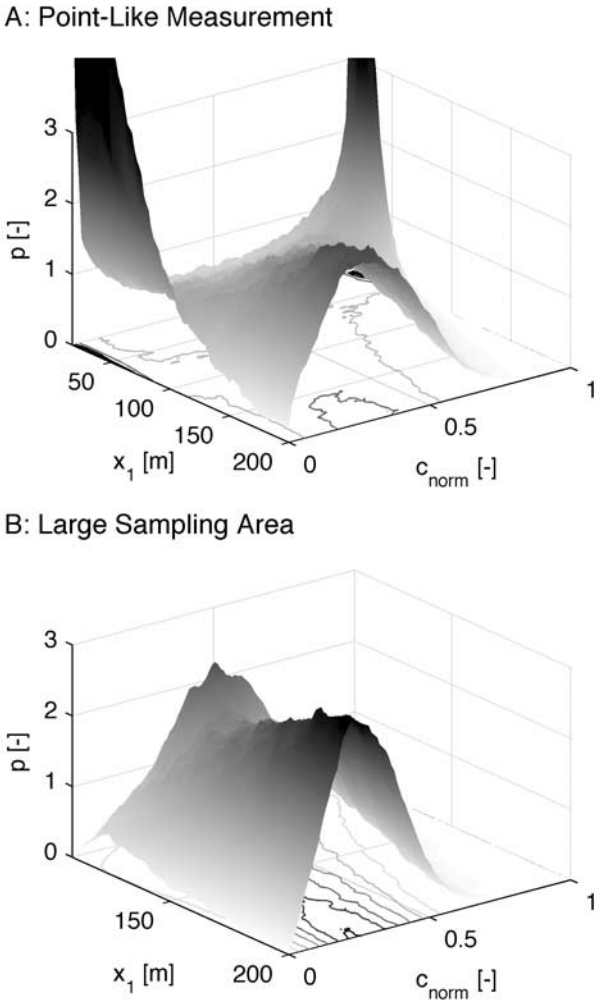

Figure 7. Steady state concentration pdf according to numerical Monte Carlo simulations. Development along the observation path from 20 m to 200 m distance to the solute source. Large transverse Péclet numbers (Pe_2 = 25,000 and Pe_3 = 12,500). (a) Point-like measurements and (b) sampling area 5.33 m × 5.33 m.

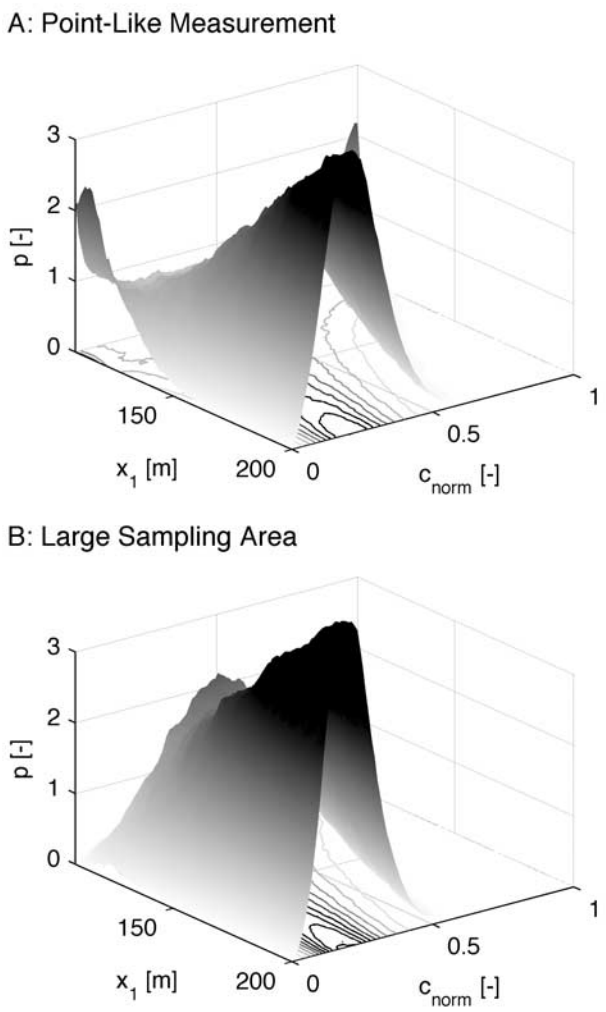

Figure 8. Steady state concentration pdf according to numerical Monte Carlo simulations. Development along the observation path from 20 m to 200 m distance to the solute source. Small transverse Péclet numbers ($Pe_2 = 250$ and $Pe_3 = 125$). (a) Point-like measurements and (b) sampling area 5.33 m × 5.33 m.

[62] Generally, the pdf's of both methods agree reasonably. We conclude that the semianalytical approach approximates the distribution of concentration quite well. Nonetheless, we observe a few basic differences. It seems that the peaks of the concentration pdf at the extreme values are systematically lower in the numerical results than in the semianalytical ones. Consequently, the peaks at intermediate concentration values are more pronounced in the numerical simulations than in the semianalytical approach. In cases where the concentration pdf is unimodal, the peak of the semianalytical approach tends to be shifted toward smaller concentrations in comparison to the numerical results. As mentioned above, multimodal pdf's, exhibiting three peaks, are seldom observed in the numerical calculations.

[63] With exception of the point-like observation (see Figure 11a), the difference between the two approaches is larger for small travel distance ($x_1 = 2\lambda_1$) than for large travel distance ($x_1 = 16\lambda_1$). The reasons for this discrepancy are manifold. *Dagan* [1989] and *Rubin* [2003] report, that even the (ensemble) mean concentration does not have a Gaussian shape along cross sections at small travel distances in cases where the log conductivity variance σ_Y^2 exceeds values of 0.05. To the best of our knowledge, there are no studies on the shape of individual plumes in cross sections, but it seems reasonable to assume that they even less resemble Gaussian distributions. Another reason might be that we calculate the dispersion tensor only to first order accuracy, which may be insufficient for the transverse components [*Dentz et al.*, 2002; *Attinger et al.*, 2004]. For example, flow focussing in high-conductivity areas enhances solute mixing [*Werth et al.*, 2006], which is a higher-order effect. Furthermore, we cannot exclude that numerical dispersion affects the results of the numerical Monte Carlo simulations.

[64] For larger travel distances, the results of the two methods become similar (see Figure 11), except for the above described shifting of the peak in the semianalytical

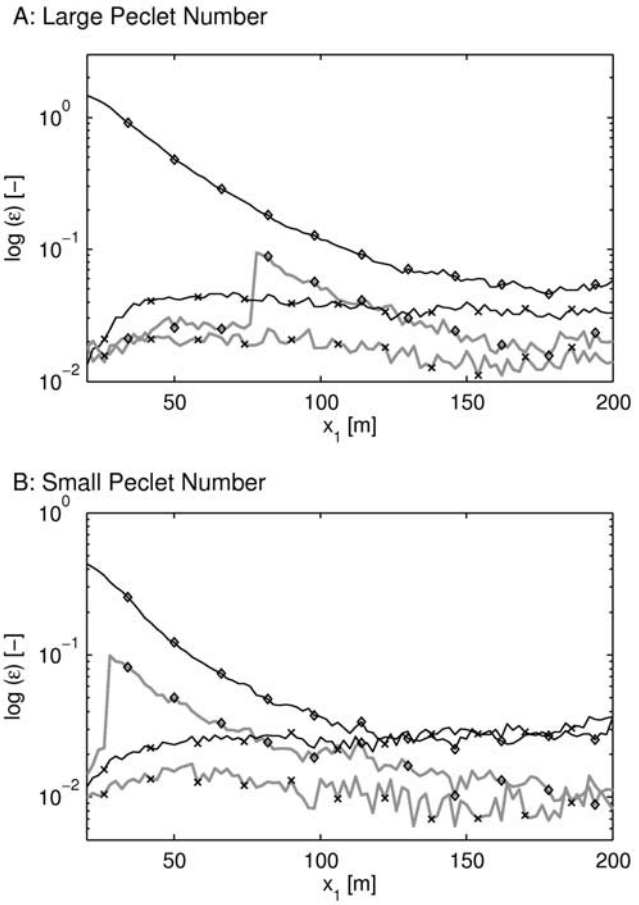

Figure 9. Fitting error ε according to equation (38) of the Gaussian fit (black line) and the beta fit (gray line) compared to the numerical results as function of travel distance. Diamonds indicate point-like measurements, and crosses indicate sampling area 5.33 m × 5.33 m. (a) Large transverse Péclet numbers ($Pe_2 = 25{,}000$ and $Pe_3 = 12{,}500$) and (b) small transverse Péclet numbers ($Pe_2 = 250$ and $Pe_3 = 125$).

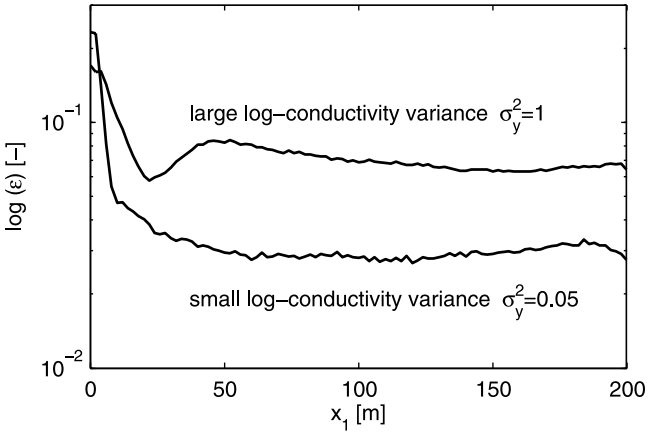

Figure 10. Root-mean-square error ε between the semianalytical and the numerical approaches for point-like measurements and log conductivity variance $\sigma_Y^2 = 0.05$ and $\sigma_Y^2 = 1$, respectively. The errors are given along the observation path with different distances (x_1) to the contaminant source.

concentration pdf's toward lower concentration values. This may mean that the assumptions of the semianalytical approach are less restrictive for larger travel distances. The distance needed for the two methods to approach similar pdf's decreases with increasing sampling volume. The smoother the concentration distribution, the better the two approaches agree. Smoothing can be achieved either by increasing the sampling volume, or by letting dispersion act over a longer travel time.

5. Conclusions

[65] In this study, we have analyzed how increasing the sampling volume affects the probability density function of steady state concentration in heterogeneous formations. *Fiorotto and Caroni* [2002] and *Caroni and Fiorotto* [2005] had already shown that point-like concentration measurements exhibit a bimodal pdf at short travel distance. With increasing travel distance, the measurement device samples a larger fraction of the inflow plane which leads to a decrease in concentration variance and a unimodal pdf of concentration. Increasing the sampling area has a similar effect. The larger the sampling area, the shorter is the travel distance over which multimodal behavior can be observed.

[66] We have presented a semianalytical approach of computing the full statistical distribution of concentrations sampled over a rectangular area in second-order stationary velocity fields. Application to other source and sampling volume geometries is straightforward. Relying on first-order stochastic theory of effective dispersion, our approach cannot take into account higher-order effects, such as enhanced transverse mixing due to flow focusing [*Werth et al.*, 2006]. Conversely, the evaluation of the concentration pdf by numerical Monte Carlo simulations used for comparison is computationally demanding and may be compromised by numerical dispersion.

[67] The shape of the concentration pdf is of significance in risk assessment, in the transfer to reactive transport [*Cirpka et al.*, 2008], and in statistical inference [*Michalak and Kitanidis*, 2003]. Our results confirm that quasi-Gaussian statistical distributions are obtained either after passing long travel distances or by averaging over large sampling volumes. If the expected value and variance of

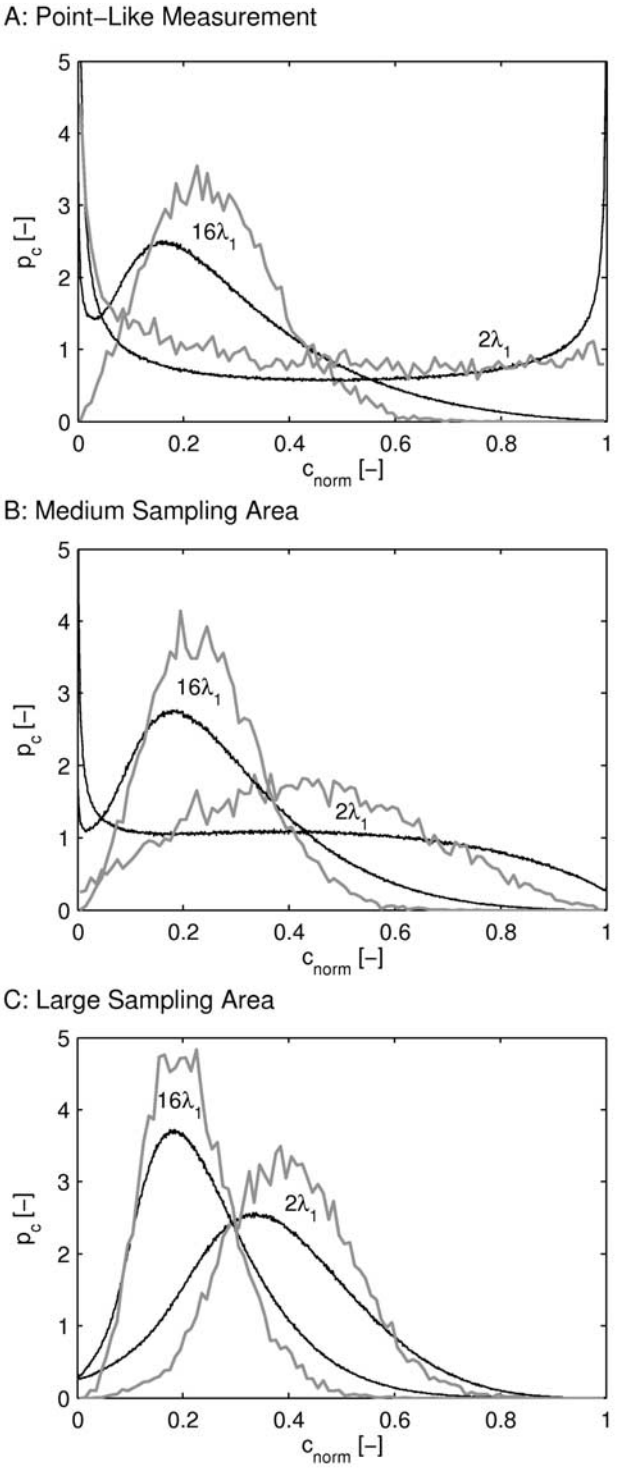

Figure 11. Comparison of the semianalytical (black line) and numerical (gray line) concentration pdf's for log conductivity variance $\sigma_Y^2 = 1$. (a) Point-like measurement, (b) sampling area 4 m × 4 m, and (c) sampling area 8 m × 8 m.

concentration are the only available information, we recommend assuming a beta distribution for the concentration pdf rather than relying on low-order perturbation approaches in propagating uncertainty from log-conductivity or velocity to concentrations, which implicitly assume Gaussian distributions.

Appendix A: Derivation of Equation (15)

[68] For the derivation of equation (15), we start with the weak form of equation (1) subject to the boundary conditions given in equation (2). Multiplying equation (1) with a test function ψ and integrating over the spatial domain yields:

$$\int_{\Omega} \psi \boldsymbol{\nabla} \cdot (\boldsymbol{v}c - \boldsymbol{D}\boldsymbol{\nabla}c)\,\mathrm{d}\boldsymbol{x} = 0, \tag{A1}$$

subject to the boundary conditions:

$$\begin{aligned} \int_{\Gamma_{\mathrm{in}}} \boldsymbol{n} \cdot (\psi \boldsymbol{v}c - \psi \boldsymbol{D}\boldsymbol{\nabla}c)\,\mathrm{d}\boldsymbol{x} &= \int_{\Gamma_{\mathrm{in}}} \boldsymbol{n} \cdot \psi \boldsymbol{v}c_{in}\,\mathrm{d}\boldsymbol{x} \\ \int_{\Gamma_{\mathrm{out}} \cup \Gamma_{\mathrm{no}}} \boldsymbol{n} \cdot (\psi \boldsymbol{D}\boldsymbol{\nabla}c)\,\mathrm{d}\boldsymbol{x} &= 0. \end{aligned} \tag{A2}$$

[69] Applying Green's theorem to equation (A1) results in

$$\begin{aligned} &\int_{\Omega} (-\boldsymbol{\nabla}\psi \cdot \boldsymbol{v} - \boldsymbol{\nabla} \cdot (\boldsymbol{D}\boldsymbol{\nabla}\psi))c\,\mathrm{d}\boldsymbol{x} \\ &\quad + \int_{\Gamma} n \cdot (\psi \boldsymbol{v}c - \psi \boldsymbol{D}\boldsymbol{\nabla}c + \boldsymbol{\nabla} \cdot (\psi \boldsymbol{D}c))\,\mathrm{d}\boldsymbol{x} = 0. \end{aligned} \tag{A3}$$

[70] Multiplying the observation equations, equations (8) and (10), for resident and flux concentration, respectively, with $\bar{v}_1^{\chi}(\mathbf{x}^{obs})$ and subtracting the result from equation (A3) leads to:

$$\begin{aligned} \int_{\Omega} \Big(& -\boldsymbol{\nabla}\psi \cdot \boldsymbol{v} - \boldsymbol{\nabla} \cdot (\boldsymbol{D}\boldsymbol{\nabla}\psi) \\ & - \chi\left(\boldsymbol{x}_{2,3} - \boldsymbol{x}_{2,3}^{obs}\right)\delta\left(x_1 - x_1^{obs}\right)\widehat{v}\Big)c\,\mathrm{d}\boldsymbol{x} \\ & + \int_{\Gamma} \boldsymbol{n} \cdot \left(\underbrace{\psi \boldsymbol{v}c}_{1} - \underbrace{\psi \boldsymbol{D}\boldsymbol{\nabla}c}_{2} + \underbrace{c\boldsymbol{D}\boldsymbol{\nabla}\psi}_{3} \right) \mathrm{d}\boldsymbol{x} = -v_1^{\chi} c_{obs}^{r/f}, \end{aligned} \tag{A4}$$

in which $\widehat{v}$ equals $\bar{v}_1\chi$ for the measurement of resident concentration, and v_1 for that of flux concentration. In equation (A4) we have dropped the argument $\boldsymbol{x}^{obs}$ in $\bar{v}_1^{\chi}(\boldsymbol{x}^{obs})$ for convenience.

[71] If ψ meets equations (13) and (12) for resident and flux concentration, respectively, subject to equation (14) we obtain the observation equation, equation (15), using the weighting function ψ. In detail: Meeting equation (13) and equation (12), respectively, eliminates the integral over the domain Ω. The integral over the boundary $\Gamma = \Gamma_{\mathrm{in}} \cup \Gamma_{\mathrm{out}} \cup \Gamma_{\mathrm{no}}$ can be considered separately. The integral of 1, 2, and 3 over Γ_{no} vanishes because of equations (14) and (A2). The integrals of 2 and 3 over Γ_{out} and Γ_{in} vanish because of equations (A2) and (14), respectively. 1 + 3 integrated over Γ_{out} vanishes because of equation (14). So finally because of equation (A2) the integral of 1 + 2 over Γ_{in} is $\int_{\Gamma_{\mathrm{in}}} \boldsymbol{n} \cdot \psi \boldsymbol{v}c_{in}\mathrm{d}\boldsymbol{x}$ by using $\boldsymbol{n} = (-1, 0, 0)^T$ on Γ_{in} we obtain equation (15).

Notation

c	concentration.
$\boldsymbol{C}_{\boldsymbol{m}_1\boldsymbol{m}_1}(t)$	covariance matrix of first spatial moments.
$\boldsymbol{C}_{\boldsymbol{m}_1\boldsymbol{m}_1;2,3}(\cdot)$	covariance matrix of first spatial moments in the transverse directions.
c_{obs}	concentration observed by the semi-analytical method.
$c_{\mathrm{obs}}^{p}(\boldsymbol{\xi}_{2,3}, v_{rel})$ and $c_{\mathrm{obs}}^{SV}(\boldsymbol{\xi}_{2,3}, v_{rel})$	observed concentration for point-like measurements and larger sampling volume, respectively.
c_{obs}^{r}, c_{obs}^{f}	observed resident and flux concentration, respectively.
$c_{\mathrm{obs}}^{\mathrm{tar}}$	target concentration for cdf threshold.
c_{sim}	concentration simulated by the numerical MC method.
$\boldsymbol{D}$	dispersion tensor.
$\boldsymbol{D}^*$	ensemble dispersion tensor.
$\boldsymbol{D}^e$	effective dispersion tensor.
$\mathrm{E}(\cdot)$	expected value.
f	continuous pdf of a parametric distribution.
$\widehat{F}_c^{ana}(c_{\mathrm{obs}}^{\mathrm{tar}})$	empirical cumulative distribution function for a given target concentration $c_{\mathrm{obs}}^{\mathrm{tar}}$ of the semianalytical results.
$f_{\mathcal{B}(\alpha,\beta)}(x)$	pdf of the beta distribution.
$\widehat{f}_h(c)$	empirical pdf of a empirical cdf as histogram.
$\widehat{F}_c^{num}(c_{\mathrm{obs}}^{\mathrm{tar}})$	empirical cumulative distribution function for a given target concentration $c_{\mathrm{obs}}^{\mathrm{tar}}$ of the numerical MC results.
$F_{v_{rel}}(v_{rel})$	cdf of v_{rel}.
h	hydraulic heads.
i	imaginary unit.
K, Y	hydraulic conductivity, hydraulic log-conductivity.
$\boldsymbol{m}_1(t)$	first spatial moment.
Pe_2, Pe_3	Péclet number in transverse directions.
$R_{v_1v_1}(\boldsymbol{h})$	autocovariance function of the longitudinal velocity component with distance vector $\boldsymbol{h}$.
$R_{Y'Y'}(\lvert\boldsymbol{x} - \boldsymbol{z}\rvert)$	covariance function of the log-conductivity field for an exponential model.
$\boldsymbol{S}_{\boldsymbol{v}'\boldsymbol{v}'^T}$	power spectrum of the velocity fluctuations.
$\mathrm{sinc}(\cdot)$	normalized sinc function.
$\boldsymbol{S}_{Y'Y'^T}$	power spectrum of the log-conductivity fluctuations.
t,τ	time variables.
$\boldsymbol{v} = (v_1, v_2, v_3)^T$	seepage velocity.
$\bar{\boldsymbol{v}} = (\bar{v}_1, \bar{v}_2, \bar{v}_3)^T$	mean value of seepage velocity.
v_{rel}	relative velocity (see equation (17)).
$v_{rel}\psi^{p}(\boldsymbol{x}'_{2,3}\lvert\boldsymbol{\xi}_{2,3})$ and $v_{rel}\psi^{SV}(\boldsymbol{x}'_{2,3}\lvert\boldsymbol{\xi}_{2,3})$	distribution of relative velocity times weighting function for point-like and for larger sampling areas, respectively.
$V_{\boldsymbol{y}}$	domain of the Fourier space.

$\bar{v}_1^{\chi}(\boldsymbol{x}^{obs})$ mean longitudinal velocity in the sampling area (see equation (11)).

w_2, w_3 width in x_2 and x_3 direction, respectively.

$\boldsymbol{x} = (x_1, x_2, x_3)^T$ spatial coordinate vector.

$\boldsymbol{x}' = (x'_1, x'_2, x'_3)^T$ spatial coordinate vector in the inflow plane.

$\boldsymbol{x}_{2,3} = (x_2, x_3)^T$ transverse spatial coordinate vector.

$\boldsymbol{x}^{obs}$ spatial coordinate vector.

$\boldsymbol{y} = (y_1, y_2, y_3)^T$ spectral coordinate.

$\Gamma = \partial\Omega$ boundary of the spatial domain.

$\Gamma(z)$ Gamma function.

$\Delta\boldsymbol{M}_{2c}(\mathrm{E}[c(t)])$ change of second central spatial moments of the ensemble concentration.

$\Delta\boldsymbol{\Xi}(t)$ difference of the expected value of second central spatial moments.

$\Delta\Xi_{ij}(t)$ element i,j of matrix $\Delta\boldsymbol{\Xi}(t)$.

$\varepsilon^2(\widehat{f}_h, f)$ error measure for the distance between a stepwise constant empirical pdf $\widehat{f}_h(c)$ within the unit domain and a continuous parametric pdf $f(c)$.

$\boldsymbol{\lambda} = (\lambda_1, \lambda_2, \lambda_3)^T$ vector of correlation length.

$\boldsymbol{\xi}_{2,3} = (\xi_2, \xi_3)^T$ first transverse moments of the weighting function ψ in the injection plane.

$\sigma^2_{v_{rel}}$ variance of v_{rel}.

σ^2_Y variance of the log-conductivity field.

$\chi(\boldsymbol{x})$ $\tilde{\chi}(\boldsymbol{y})$ and sampling function and its Fourier transform.

ψ weighting function (adjoint concentration).

Ω spatial domain.

$\cdot \otimes \cdot$ tensor product.

[72] **Acknowledgments.** This study has been funded by the Swiss National Science Foundation (SNF) under grant 20021-109169. Additional support has been provided by Deutsche Forschungsgemeinschaft under grant 824/3-1.

References

Andričević, R. (1998), Effects of local dispersion and sampling volume on the evolution of concentration fluctuations in aquifers, *Water Resour. Res.*, *34*(5), 1115–1129.

Attinger, S., M. Dentz, and W. Kinzelbach (2004), Exact transverse macro dispersion coefficients for transport in heterogeneous porous media, *Stochastic Environ. Res. Risk Assess.*, *18*(1), 9–15.

Bakr, A. A., L. W. Gelhar, A. L. Gutjahr, and J. R. MacMillan (1978), Stochastic analysis of spatial variability in subsurface flows: 1. Comparison of one-dimensional and three-dimensional flows, *Water Resour. Res.*, *14*(2), 263–271.

Beckie, R. (1996), Measurement scale, network sampling scale, and groundwater model parameters, *Water Resour. Res.*, *32*(1), 65–76.

Bellin, A., and D. Tonina (2007), Probability density function of nonreactive solute concentration in heterogeneous porous formations, *J. Contam. Hydrol.*, *94*(1–2), 109–125, doi:10.1016/j.jconhyd.2007.05.005.

Brooks, A. N., and T. J. R. Hughes (1982), Streamline upwind Petrov-Galerkin formulations for convection dominated flows with particular emphasis on the incompressible Navier-Stokes equations, *Comput. Methods Appl. Mech. Eng.*, *32*(1–3), 199–259.

Caroni, E., and V. Fiorotto (2005), Analysis of concentration as sampled in natural aquifers, *Transp. Porous Media*, *59*(1), 19–45.

Cirpka, O. A., and P. K. Kitanidis (2000), Characterization of mixing and dilution in heterogeneous aquifers by means of local temporal moments, *Water Resour. Res.*, *36*(5), 1221–1236.

Cirpka, O. A., and A. J. Valocchi (2007), Two-dimensional concentration distribution for mixing-controlled bioreactive transport in steady state, *Adv. Water Resour.*, *30*(6–7), 1668–1679.

Cirpka, O. A., R. L. Schwede, J. Luo, and M. Dentz (2008), Concentration statistics for mixing-controlled reactive transport in random heterogeneous media, *J. Contam. Hydrol.*, *98*(1–2), 61–74.

Dagan, G. (1984), Solute transport in heterogeneous porous formations, *J. Fluid Mech.*, *145*, 151–177.

Dagan, G. (1989), *Flow and Transport in Porous Formations*, Springer, Berlin.

Dentz, M., H. Kinzelbach, S. Attinger, and W. Kinzelbach (2000a), Temporal behavior of a solute cloud in a heterogeneous porous medium 1. Point-like injection, *Water Resour. Res.*, *36*(12), 3591–3604.

Dentz, M., H. Kinzelbach, S. Attinger, and W. Kinzelbach (2000b), Temporal behavior of a solute cloud in a heterogeneous porous medium: 2. Spatially extended injection, *Water Resour. Res.*, *36*(12), 3605–3614.

Dentz, M., H. Kinzelbach, S. Attinger, and W. Kinzelbach (2002), Temporal behavior of a solute cloud in a heterogeneous porous medium 3. Numerical simulations, *Water Resour. Res.*, *38*(7), 1118, doi:10.1029/2001WR000436.

De Simoni, M., X. Sanchez-Vila, J. Carrera, and M. W. Saaltink (2007), A mixing ratios-based formulation for multicomponent reactive transport, *Water Resour. Res.*, *43*, W07419, doi:10.1029/2006WR005256.

Dietrich, C. R., and G. N. Newsam (1993), A fast and exact method for multidimensional gaussian stochastic simulations, *Water Resour. Res.*, *29*(8), 2861–2869.

Eberhard, J. (2004), Approximations for transport parameters and self-averaging properties for point-like injections in heterogeneous media, *J. Phys. A Math. Gen.*, *37*(7), 2549–2571, doi:10.1088/0305-4470/37/7/003.

Englert, A., J. Vanderborght, and H. Vereecken (2006), Prediction of velocity statistics in three-dimensional multi-Gaussian hydraulic conductivity fields, *Water Resour. Res.*, *42*, W03418, doi:10.1029/2005WR004014.

Fiori, A., and G. Dagan (2000), Concentration fluctuations in aquifer transport: A rigorous first-order solution and applications, *J. Contam. Hydrol.*, *45*(1–2), 139–163.

Fiori, A., S. Berglund, V. Cvetkovic, and G. Dagan (2002), A first-order analysis of solute flux statistics in aquifers: The combined effect of pore-scale dispersion, sampling, and linear sorption kinetics, *Water Resour. Res.*, *38*(8), 1137, doi:10.1029/2001WR000678.

Fiorotto, V., and E. Caroni (2002), Solute concentration statistics in heterogeneous aquifers for finite Peclet values, *Transport Porous Media*, *48*, 331–351, (Erratum, *Transp. Porous Media*, *50*(3), 373, 2003.)

Gelhar, L. W., and C. L. Axness (1983), Three-dimensional stochastic-analysis of macrodispersion in aquifers, *Water Resour. Res.*, *19*(1), 161–180.

Graham, W., G. Destouni, G. Demmy, and X. Foussereau (1998), Prediction of local concentration statistics in variably saturated soils: Influence of observation scale and comparison with field data, *J. Contam. Hydrol.*, *32*(1–2), 177–199.

Gutjahr, A. L., L. W. Gelhar, A. A. Bakr, and J. R. MacMillan (1978), Stochastic analysis of spatial variability in subsurface flows: 2. Evaluation and application, *Water Resour. Res.*, *14*(5), 953–959.

Kapoor, V., and L. W. Gelhar (1994), Transport in three-dimensionally heterogeneous aquifers: 1. Dynamics of concentration fluctuations, *Water Resour. Res.*, *30*(6), 1775–1788.

Kitanidis, P. K. (1988), Prediction by the method of moments of transport in a heterogeneous formation, *J. Hydrol.*, *102*(1–4), 453–473.

Kitanidis, P. K. (1995), Quasi-linear geostatistical theory for inversing, *Water Resour. Res.*, *31*(10), 2411–2419.

Li, S. G., and D. McLaughlin (1991), A nonstationary spectral method for solving stochastic groundwater problems: Unconditional analysis, *Water Resour. Res.*, *27*(7), 1589–1605.

Li, S. G., and D. McLaughlin (1995), Using the nonstationary spectral method to analyze flow-through heterogeneous trending media, *Water Resour. Res.*, *31*(3), 541–551.

Liu, G. S., Z. M. Lu, and D. X. Zhang (2007), Stochastic uncertainty analysis for solute transport in randomly heterogeneous media using a Karhunen-Loeve-based moment equation approach, *Water Resour. Res.*, *43*(7), W07427, doi:10.1029/2006WR005193.

Lu, Z. M., and D. X. Zhang (2004), Comparative study on uncertainty quantification for flow in randomly heterogeneous media using Monte Carlo simulations and conventional and KL-based moment-equation approaches, *SIAM J. Sci. Comput.*, *26*(2), 558–577.

Michalak, A. M., and P. K. Kitanidis (2003), A method for enforcing parameter nonnegativity in Bayesian inverse problems with an application to contaminant source identification, *Water Resour. Res.*, *39*(2), 1033, doi:10.1029/2002WR001480.

Neuman, S. P. (1993), Eulerian-langrangian theory of transport in space-time nonstationary velocity fields: Exact nonlocal formalism by conditional moments and weak approximation, *Water Resour. Res.*, *29*(3), 633–645.

Neuman, S. P., and S. Orr (1993), Prediction of steady-state flow in nonuniform geologic media by conditional moments: Exact nonlocal formalism, effective conductivities, and weak approximation, *Water Resour. Res.*, *29*(2), 341–364.

Neuman, S. P., C. L. Winter, and C. M. Newman (1987), Stochastic-theory of field-scale fickian dispersion in anisotropic porous-media, *Water Resour. Res.*, *23*(3), 453–466.

Neupauer, R. M., and J. L. Wilson (1999), Adjoint method for obtaining backward-in-time location and travel time probabilities of a conservative groundwater contaminant, *Water Resour. Res.*, *35*(11), 3389–3398.

Nowak, W., R. L. Schwede, O. A. Cirpka, and I. Neuweiler (2008), Probability density functions of hydraulic head and velocity in three-dimensional heterogeneous porous media, *Water Resour. Res.*, *44*, W08452, doi:10.1029/2007WR006383.

Pope, S. B. (1985), Pdf methods for turbulent reactive flows, *Prog. Energy Combust. Sci.*, *11*(2), 119–192.

Rubin, Y. (2003), *Applied Stochastic Hydrogeology*, Oxford Univ. Press, Oxford, U.K.

Rubin, Y., A. Sun, R. Maxwell, and A. Bellin (1999), The concept of block-effective macrodispersivity and a unified approach for grid-scale- and plume-scale-dependent transport, *J. Fluid Mech.*, *395*, 161–180.

Stüben, K. (2001), A review of algebraic multigrid, *J. Comput. Appl. Math.*, *128*(1–2), 281–309.

Sun, N., and W. Yeh (1990), Coupled inverse problems in groundwater modeling: 1. Sensitivity analysis and parameter identification, *Water Resour. Res.*, *26*(10), 2507–2525.

Werth, C. J., O. A. Cirpka, and P. Grathwohl (2006), Enhanced mixing and reaction through flow focusing in heterogeneous porous media, *Water Resour. Res.*, *42*, W12414, doi:10.1029/2005WR004511.

Zhang, D. X. (1998), Numerical solutions to statistical moment equations of groundwater flow in nonstationary, bounded, heterogeneous media, *Water Resour. Res.*, *34*(3), 529–538.

Zhang, D. X., and Z. M. Lu (2004), An efficient, high-order perturbation approach for flow in random porous media via Karhunen-Loeve and polynomial expansions, *J. Comput. Phys.*, *194*(2), 773–794.

O. A. Cirpka and R. L. Schwede, Center for Applied Geoscience, University of Tübingen, Sigwartstrasse 10, D-72076 Tübingen, Germany. (olaf.cirpka@uni-tuebingen.de; ronnie.schwede@ifg.uni-tuebingen.de)

I. Neuweiler, Institut für Strömungsmechanik, Leibniz Universität Hannover, Appelstrasse 9a, D-30167 Hannover, Germany. (neuweiler@hydromech.uni-hannover.de)

W. Nowak, Department of Civil and Environmental Engineering, University of California, 670 Davis Hall, Berkeley, CA 94720-1710, USA. (wolfgang.nowak@berkeley.edu)